Applied Geochemistry 184 (2025) 106363

Contents lists available at ScienceDirect

Applied Geochemistry

journal homepage: www.elsevier.com/locate/apgeochem

Comparison of naturally altered archaeological glasses from a marine environment with accelerated laboratory tests; implications for modelling long-term corrosion

Clare L. Thorpe [a,*], Nick Aldred [b], Stuart Creasey-Gray [a], Martin C. Stennett [a], Eperke A. Rencz [a], Susan Nehzati [c], Latham T. Haigh [a], Garry Manifold [a], Nishta Vallo [a], Christoph Lenting [d], Claire L. Corkhill [e], Russell J. Hand [a]

[a] Department of Materials Science and Engineering, University of Sheffield, S1 3JD, UK
[b] School of Life Sciences, University of Essex, CO4 3SQ, UK
[c] I18 Diamond Light Source, Fermi Ave, Didcot, OX11 0DE, UK
[d] Institut für Geologie und Mineralogie, Universitat Köln, D-50674, Germany
[e] School of Earth Sciences, University of Bristol, BS8 1RL, UK

ARTICLE INFO

Editorial handling by: Adrian Bath

Keywords:
Glass durability
Glass alteration
Natural analogues
Shipwrecks
Radioactive waste disposal
Nuclear waste

ABSTRACT

Glass ingots of lead silicate composition from the shipwreck of the *Albion* were studied to ascertain the chemistry and mineralogy of alteration products after exposure to seawater for 220 years. Alteration observed on natural samples was compared to that of the same glasses exposed to short-term, high temperature, laboratory dissolution tests in synthetic seawater and significant differences were observed. Alteration layers on natural samples were more chemically complex having sequestered high concentrations of elements present only at trace quantities in seawater. Electron microprobe analysis and microfocus x-ray absorption spectroscopy shows that P, most likely released by biological activity in the vicinity of the wreck, accumulated in naturally altered samples to form Pb–Ca-phosphate phases whilst Pb-sulphate phases formed in laboratory tests. Meanwhile Fe, present at < 0.3 wt % in the glass and ppb concentrations in seawater, accumulated to form Fe-silicates whilst Mg-silicates predominated in laboratory tests. Biologically induced corrosion of naturally altered samples was also considered. Experiments conducted to test barnacle settlement rates suggest that biotoxic elements within the glass, primarily Pb but potentially also Cu, Co and Ni deterred barnacle settlement. Despite this toxicity, some colonisation of the glass surface by both barnacles and bryozoan did occur and, whilst barnacles appeared to protect against chemical attack, bryozoan colonies caused increased cracking, possibly due stress created at the glass surface. Results highlight the challenges in recreating open, natural systems in laboratory settings and demonstrate that elements present at low concentrations can have a significant impact over long timescales.

1. Introduction

The long term behaviour of glass in an aqueous environment is of interest to materials scientists, archaeologists, biologists, artists, engineers and others. Current understanding of glass dissolution rates and mechanisms has been derived primarily from laboratory testing, typically conducted under static, sterile conditions, in closed systems and using simplified solutions (e.g. Thorpe et al., 2021; Gin et al., 2021). Meanwhile, computational models, by necessity, tend to reduce the complexity even further by simulating an idealised solid-solution interface for simple glasses (usually containing just a few elements) in simple solutions (e.g. Strachan, 2001; Ma et al., 2017; Frugier et al., 2018). Both standardised tests and models contain assumptions and require validation against real world systems. Validation is never more important that when attempting to predict the behaviour of materials or systems over timescales longer than a human lifespan where real-time testing is impractical; for example, when estimating the long-term behaviour of glassy wasteforms designed to contain radioactive elements over a million years. In this case real-time experiments are impossible, so short-term accelerated tests have been used to gain a

* Corresponding author.
E-mail address: clare.thorpe@sheffield.ac.uk (C.L. Thorpe).

https://doi.org/10.1016/j.apgeochem.2025.106363
Received 1 November 2024; Received in revised form 6 March 2025; Accepted 17 March 2025
Available online 18 March 2025

mechanistic understanding of alteration processes (e.g. by increasing the temperature and surface area to volume ratio (SA/V) (ASTM, 2021a, 2021b, 2021c).

By oversimplifying complex natural systems there is a risk of excluding minor components, slow chemical reactions, or other processes deemed negligible in a closed system in the short-term that, in an open system, may have a cumulative effect over the long-term. For example, trace elements present either in the glass or in solution can accumulate in the alteration layers over time changing their passivating properties and affecting the rate of glass alteration. In short-term dissolution experiments common groundwater constituents (i.e Na, Fe, Ca) have already been shown to affect dissolution rates when added at elevated quantities (e.g. Jollivet et al., 2012; Michelin et al., 2013; Arena et al., 2016; Arena et al., 2017; Arena et al., 2018; Corkhill et al., 2022). Natural analogue studies, where glasses have been exposed to an open 'natural' environment for long periods of time, may be especially useful in identifying minor components or processes occurring in a complex system that are likely to be significant over long time periods.

The desire to understand man-made glass behaviour, and in particular vitrified waste behaviour, has led to a rise in the study of natural glasses (e.g. volcanic basaltic and rhyolitic glasses) or anthropogenic archaeological glasses (e.g. Roman and medieval artefacts) (Miller et al., 2011; Poinssot and Gin, 2012; McCloy et al., 2019; Reijonen et al., 2023; Marcial et al., 2024). The most desirable analogues are those where the ancient glass and environment are chemically similar to the modern glass and environment of interest, and where the alteration environment is well constrained. As some modern glasses (e.g. borosilicates) have only been manufactured in the last century, the majority of analogues fall short of this criteria. Nevertheless, imperfect analogues, silicate glasses for which the composition and alteration environment are known, can still be useful in studying long-term glass corrosion mechanisms and in validating the results of laboratory dissolution tests.

Glasses recovered from shipwrecks often have the benefit that the date they were first exposed to seawater, the date the ship sunk, is noted in historical records along with the date any glass artefact was recovered. Furthermore, the chemical composition of seawater remains relatively stable and, in many parts of the world, has been monitored for the purpose of understanding marine ecosystems and climate change. Highly saline conditions, whilst not representative of many shallow subsurface groundwaters, also have some relevance to disposal scenarios in deep subsurface brines or salt formations (e.g. EPA, 2021; Nuclear Waste Services, 2023).

Chemical studies of shipwreck glasses have been conducted to understand the provenance of archaeological artefacts (e.g Stuart, 1991; Jackson and Nicholson, 2010) and/or their corrosion behaviour (e.g. Cox and Ford, 1989; Dal Bianco et al., 2004; Carmona et al., 2005; Silvestri et al., 2005; Benedetti et al., 2007; Anastassiades and Ellis, 2008; Silvestri et al., 2008; Strachan et al., 2014; Ortega-Feliu, 2016). Experiments suggest that most glasses dissolve more quickly in seawater than freshwater or sediment systems, but more slowly than in deionised water often used in laboratory tests (Dal Bianco et al., 2004; Palomar and Llorente, 2016). In one study, Verney-Carron et al. (2010) concluded that external cracks around the outer edges of a Roman glass block, exposed to constantly renewed seawater, were altered at a rate comparable to the forward rate of glass measured in the laboratory whilst internal cracks altered more slowly. They calculated the activation energy of the archaeological glass dissolution in seawater to be 76.5 kJ mol^{-1}, comparable to that of the French nuclear waste glass SON68 in pure water (71 kJ mol^{-1}) and basaltic glass (72.4 kJ mol^{-1}) (Techer et al., 2000). Alteration products, hydrated glass, smectites and carbonates, were also found to be comparable to secondary phases predicted by geochemical models.

Here, glasses from the shipwreck of the East Indiaman sailing vessel the *Albion*, sunk off Margate UK in 1765 and recovered from the wreck in 1985 and thus exposed to seawater for 220 years, were studied. The glass ingots were potash-lead-silica glasses with compositions similar to those used in 17th/18th century China. Therefore, taking account of historical context, they were likely en-route for use in Chinese glassworks (Redknap and Freestone, 1995). Reports indicate that 'hundreds' of glass ingots were found at the site of the Albion wreck but no details are provided about their stowage onboard which could impact exposure conditions (Redknap and Freestone, 1995).

Alteration observed on glass samples exposed to natural seawater was then compared to alteration in tests conducted under simple laboratory dissolution conditions in order to assess the validity of using simple systems to replicate complex natural environments. Particular attention was given to biological induced corrosion and the role of poorly soluble elements (e.g. Fe) and trace species from solution (e.g. PO_4^{3-}) in controlling alteration layer chemistry and morphology.

2. Methods

2.1. Analysis of original glass samples

Six glass ingots were donated to the University of Sheffield from a private collection whilst twelve additional ingots, from the same cargo, are held at the British Museum. Early storage history of glass ingots is not known but since arrival at Sheffield the glasses were stored in a dry cardboard box wrapped in bubble wrap. It is highly likely that some altered material has been removed by desiccation and abrasion during storage and handling. Prior to sectioning, ingots were photographed to record surface appearance and the remains of biological growth. The colonised area of each ingot was calculated using ImageJ (Image Processing and Analysis in Java). Images were uploaded, converted to grayscale and background subtracted so the program recognised as much of the biological material as possible as white. Images were then converted to a mask in order to measure the percentage of the image/glass specimens surface that was colonised by barnacles and bryozoan colonies (Fig. 1).

The topography of the surface of the glass ingots were imaged by Vertical Scanning Interferometry (VSI) using a Bruker Contour Elite microscope with green light to determine surface roughness and evidence localised corrosion (e.g. pitting). Following surface analysis, preserving as much of the samples as possible, a portion roughly 5 cm by 10 cm was removed from each ingot using a diamond tipped slow saw lubricated with water. These portions were further divided, mounted epoxy (Buehler EpoxiCure 2) and polished to a 1-μm finish before imaging in cross section. To ascertain the chemical composition of each sample a fixed mass of fine powdered glass was dissolved in acid (HF/HNO_3), diluted and then measurement by Inductively Coupled Plasma – Optical Emission Spectrometry (ICP-OES). This composition was later cross-checked against EPMA and EDX data (both assumed to be less accurate). Glass density was measured using helium pycnometry.

Cross sections were imaged by scanning electron microscopy with energy dispersive x-ray spectroscopy (SEM- EDS on an FEI Nova NanoSEM 450) and then the largest area of alteration found on Glass 5 was further investigated using and electron microprobe with wavelength dispersive x-ray spectroscopy (EPMA on a JEOL JXA 8530F). EPMA maps were taken at magnification × 2000, 10 keV, 50 nA, with dwell time 70.00 ms, interval 0.20 μm and elemental abundance was calculated in atom % and conc % (relative concentration by mass).

Microfocus x-ray fluorescence spectroscopy (μXRF), microfocus Fe K-edge x-ray absorption near-edge spectroscopy (μXANES) and (μEXAFS) was performed (on the same area as for EPMA) at the microfocus spectroscopy beamline 4-BM at NSLS (USA). An iron foil was measured at intervals to check for beam drift. Spectra were collected in fluorescence mode with a beam diameter of 2 μm. XANES spectra were collected from ~60 eV below to 200 eV above the Fe K-edge (7060–7300 eV), with 0.1 eV steps in the pre-edge region (7108–7116 eV). Multiple XANES spectra were merged and background subtracted in Athena (Demeter version: 0.9.26) and Fe K-edge pre-edge features fitted using Larch using pseudo-Voigts (xraylarch version 0.9.78). For Fe K-

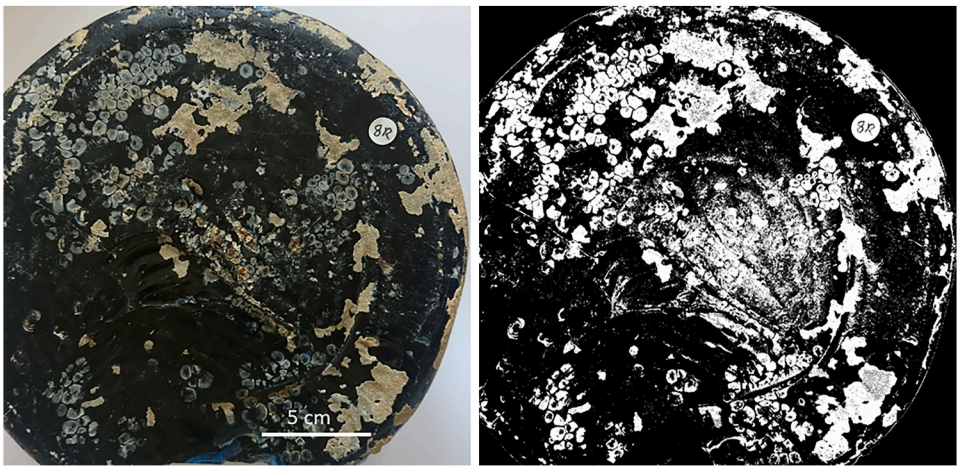

Fig. 1. (left) high resolution photograph of glass ingot 1 and (right) black and white mask created in ImageJ to calculate the area of glass colonised by biological organisms.

edge XANES, the centroid position (area-weighted average of the pre-edge peak position) of the background subtracted pre-edge and total integrated intensity of the pre-edge features were plotted against each other. Sample were compared to standard mineral phases for which the oxidation state and co-ordination number were known (Wilke et al., 2001; Farges et al., 2005; 2005, 2007).

Further μXRF, μXANES and μEXAFS was conducted on the Ca K-edge (4038 eV) and P K-edge (2152 eV) on microfocus beamline I18 at the Diamond Light Source, UK. Data was collected in fluorescence mode using a four-element Si drift detector with the sample positioned at 45° to the incident beam and a beam size of 2 μm. All Ca and P measurements were taken under a helium atmosphere to minimize X-ray absorption by the surrounding air using a bag that was constantly purged. Drift in E_0 was checked at intervals throughout the beamtime using an Fe foil and none was observed. XANES spectra for P were acquired from 2130 to 2200 eV with 0.2 eV steps close to the absorption edge and 0.1 eV energy steps over the edge. XANES spectra for Ca were acquired from 4030 to 4080 eV with 0.2 eV steps close to the absorption edge and 0.1 eV steps over the edge. Duplicate or triplicate XANES spectra were merged and background subtracted in Athena (Demeter version: 0.9.26).

2.2. Analysis of the alteration environment

Information regarding the dissolution environment in which the glass was exposed was obtained through publicly available sources from the Centre for Environment, Fisheries and Aquaculture Science (CEFAS) (Morris et al., 2016). Average temperature data were taken from the closest three monitoring points to the site of the wreck (51° 22.9' N 001° 27.2' E): Goodwin Sands (51° 13.0' N 001° 36.0 ' E; 11 nautical miles SE of the wreck), Dover (51° 07.0 ' N 001° 21.0' E; 16 nautical miles SSW of the wreck) and Tongue (51° 30.6 ' N 001° 23.0' E; 8 nautical miles NW of the wreck). Seawater chemistry was measured by the RV Corella and RV Clione throughout 1976 producing a report: "Physical and chemical properties of seawater" for the North Sea, in each month of 1976 (Morris et al., 2016). Various other databases are available through CEFAS for parameters such as temperature, phosphate concentration, nutrients, salinity and plankton for the North Sea area.

2.3. Laboratory tests

To test the relative durability of the three glasses, a modified ASTM C1285 (PCT-B) powder dissolution test was performed (ASTM, 2021b). Glass was crushed and sieved to a size fraction of 75–150 μm and subjected to a 28 day dissolution test in Type 1 - UHQ water (18 MΩ cm^{-1}), at a SA/V of 1200 and a temperature of 90 °C with sampling timepoints at 3, 7, 14, 21 and 28 days. To simulate the formation of alteration layers under marine conditions, a modified ASTM C1220 (Standard Test Method for Static Leaching of Monolithic Waste Forms for Disposal of Radioactive Waste – formally known as MCC-1) (ASTM, 2021c) test was carried out in seawater. Coupons approximately 1 cm by 1 cm by 0.5 cm were cut from the unaltered interior of each glass ingot and polished to 1-μm surface finish with diamond suspension. In the MCC-1 test, duplicate glass monoliths were exposed to synthetic seawater (Table 1) at a SA/V of 10 m^{-1} and a SA/V of 0.4 m^{-1} for time periods of 58, 112, 262 and 365 days. Both the solution and the solid glass sample were analysed at each timepoint. ICP-OES was used to measure Pb, Na, Mg, Ca, K, Sr, S, B, Fe, Pb and P in the aqueous phase whilst altered glass samples were mounted in epoxy resin (Buehler EpoxiCure 2), cross sectioned by diamond slow saw, polished to a 1μ finish and imaged by SEM with EDX and EMPA. Geochemical modelling of end point ICP-OES

Table 1
Reference Composition of seawater with practical salinity ≡ 35.000 and reference salinity ≡ 35.16504 g/kg. Units of concentration are per kilogram of seawater. Real seawater contains additional constituents (e.g. nitrates and phosphates) which are not included in the Reference Composition but whose concentrations (and their variation) may be larger than 1 mg/kg. Concentrations of these constituents do not increase or decrease with salinity but are largely controlled by biogeochemical processes.

Element	mmol/kg	mg/Kg (ppm)	Included	Reason
Na^+	468.9	10781.45	Yes	
Mg^{2+}	52.8	1283.72	Yes	
Ca^{2+}	10.3	412.08	Yes	
K^+	10.2	399.1	Yes	
Sr^{2+}	0.0907	7.94	Yes	
Cl^-	545.9	19352.71	Yes	
SO_4^{2-}	28.2	2712.35	Yes	
Br^-	0.84	67.29	Yes	
HCO_3^-	1.72	104.81	Yes	
CO_3^-	0.238	14.34	Yes	
$B(OH)_3$/$B(OH)_4$	0.314/ 0.1008	19.43/7.94	No	Possible tracer from glass
CO_2	0.0097	0.43	No	Controlled by atmosphere and temperature
OH^-	0.008	0.14	Yes	
O_2	0–0.3	0–10	No	Controlled by atmosphere and temperature
$Si(OH)_4$	0–0.17	0–16	No	Major release from glass
PO_4	0–0.003	0–0.2	Yes	Can be higher near shore
Fe		1–3 ppb	No	Below detection limits of ICP-OES

analysis was conducted in PHREEQC Version 3.7.0 using the minteq database (minteq.dat) containing thermodynamic data for the aqueous species, gas and mineral phases that are derived from the database files of MINTEQA2 (Allison et al., 1991).

2.4. Barnacle settlement experiments

A laboratory settlement assay was conducted using three-day-old cypris larvae of the barnacle *Amphibalanus improvisus*. Briefly, nauplius larvae were naturally released from adult barnacles, collected by attraction to a point light source and grown in a 2L culture containing the marine alga *Thalassiosira pseudonana* as a food source. After six nauplius stages over approximately 5 days, the larvae metamorphosed into cyprids. These were filtered from the culture using a 250 μm mesh, cleaned and stored at 4 °C for three days before use in the settlement assays. Two settlement assays were conducted, with the second including a borosilicate glass and a polystyrene standard, which the first assay lacked. A 0.5 mL droplet of artificial seawater (TropicMarin, Tropical Marine Centres, UK) was added to each of three replicate surfaces for each glass type. Into the droplet were added 10 three-day-old cyprids and the assay was stored in the dark at 28 °C for 48 h. After this time, the number of permanently settled and metamorphosed barnacles was counted, expressed as a proportion of the 10 larvae in the droplet and averaged across the three replicates of each glass type, in each assay.

3. Results and discussion

3.1. Sample characterisation

3.1.1. Chemical composition of the glasses

The six ingots made available for this study are of two shapes, rectangular (roughly 5 cm by 15 cm by 25 cm) and plano-convex (roughly 6 cm in height with a diameter of 20 cm) (Fig. 2). Biological growth observed on some ingots confirms that at least some were exposed and not buried under sediment.

Compositional analysis was performed initially by acid digestion followed by ICP-OES and later corroborated by EPMA (Table 2). Major components were SiO_2 (56–65 mol %), PbO (9–11 mol %), Al_2O_3 (1–15 mol %) and K_2O (14–17 mol %) while all other cations contribute 1 mol % oxide or less. Notable minor constituents are those used as colourants: ~1.0 % CuO (in the green glasses) and CoO ~ 0.04 % (in the blue glasses). Na_2O, MgO, CaO and Fe_2O_3 were present at very low concentrations characteristic of pre-industrial glasses (typically <0.3 %) as trace metals sourced from the potash and silica sources. These compositions are in agreement with samples held at the British museum that were analysed by XRF (Redknap et al., 1995). Densities of 3.333, 3.285 and 3.362 g cm^{-3} were measured for the blue, clear and green glasses respectively.

3.1.2. Alteration environment

The wreck of the Albion lies at latitude and longitude 51° 22.9' N 001° 27.2' E off the east coast of England close to the town of Margate (Fig. 3). Seawater monitoring has taken place intensively in the southern North Sea since 1880 with the founding of the Marine Biological Association in 1884 and the designation of Lowestoft as a 'Fisheries Laboratory' in 1902. The shipwreck of the *Albion* lies at a charted depth of 6 m and, therefore, surface temperature readings taken at a depths of 0–3 m in the vicinity of the wreck are likely to be close to seabed temperatures; seawater temperatures in the upper 'mixed' layer being relatively constant. Data from the three monitoring stations situated closest to the site of the wreck site give an annual average temperature of 11.2 °C fluctuating annually between lows of 6 °C in the winter months and 17 °C in the summertime (Fig. 3; Morris et al., 2016). Salinity measurements collected by the research vessel RV CIROLANA vary between 34.5 and 35.0 (measured by PSS-78 g/kg of seawater) (CEFAS open database). The approximate chemical composition of seawater can be taken to be close to that described in Table 1, however the concentration of dissolved organic matter and associated anions such as PO_4^{3-} may vary and generally increase with increasing biological activity.

3.1.3. Observed alteration on shipwreck samples

Localised corrosion was evident across all glass samples with preferential attack concentrated in pits and lines assumed to originate as surface defects and scratches (Fig. 4). These features had an average depth of 12.0 ± 9.8 μm measured by vertical scanning interferometry. The surface index (lateral surface area/measured surface area) was measured at 1.086 ± 0.103 (average of 27 measurements), indicating that preferential alteration at these sites led to an increase in surface area of approximately 10 % (SI Table 1). In cross section, some of these features manifested as 'vermiform', spherical tube-like pitting that has been discussed at length in the literature and summarised in Mansfield et al. (2023) (Fig. 5A and B). Other features followed the profile of scratches or cracks. In these samples, vermiform features were especially

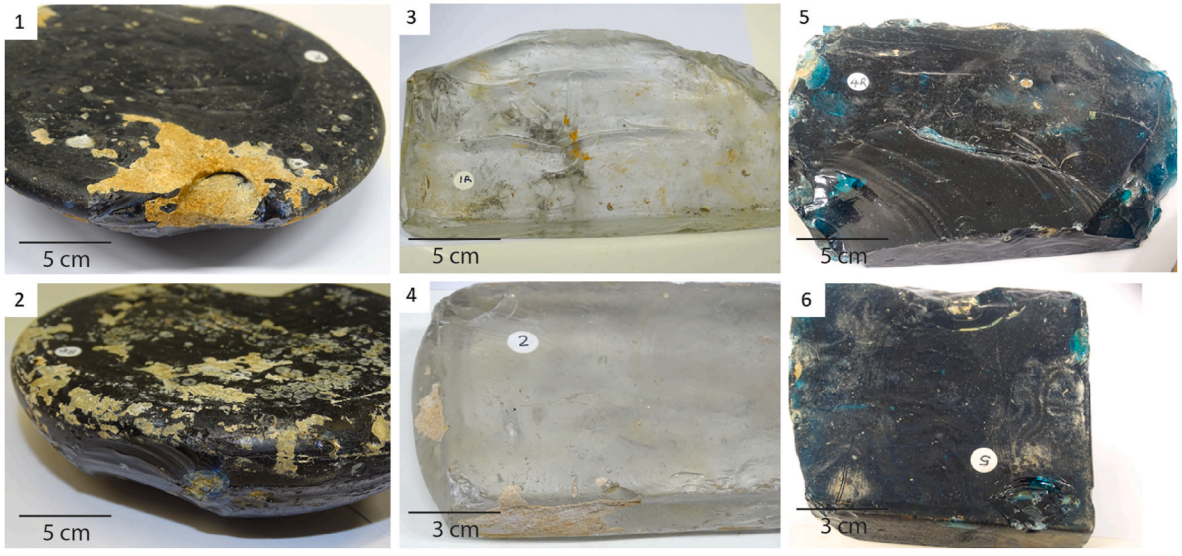

Fig. 2. Photographs of the six glass ingots coloured deep blue (1 and 2), clear (3 and 4) and green (5 and 6). Further more detailed images are provided in the supporting information (SI Figs. 1–6). (For interpretation of the references to colour in this figure legend, the reader is referred to the Web version of this article.)

Table 2
Oxide weight % (wt %) and oxide mole % (mol %) for major and minor elements in the six glasses featured in this study analysed at the University of Sheffield by acid digest followed by ICP-OES. The largest errors are obtained during the acid digestion stage and are estimated to be less than ±5 % calculated by comparison to reference material with known composition.

Glass	1 Blue		2 Blue		3 Clear		4 Clear		5 Green		6 Green	
	wt %	mol %	wt %	mol %	wt %	mol %	wt %	mol %	wt %	mol %	wt %	mol %
SiO_2	40.14	58.16	40.49	58.14	39.07	57.63	42.88	62.36	48.03	68.41	47.28	67.88
Al_2O_3	17.30	14.77	17.87	15.12	17.56	15.27	10.52	9.01	0.26	0.21	0.26	0.22
BaO	0.02	0.01	0.02	0.01	0.00	0.00	0.00	0.00	0.00	0.00	0.00	0.00
CaO	0.58	0.90	0.82	1.26	0.14	0.22	0.18	0.28	0.29	0.44	0.22	0.33
CoO	0.03	0.03	0.05	0.05	0.00	0.00	0.00	0.00	0.00	0.00	0.00	0.00
CuO	0.02	0.02	0.01	0.01	0.00	0.00	0.00	0.00	0.90	0.97	0.96	1.04
Fe_2O_3	0.50	0.27	0.49	0.27	0.11	0.06	0.11	0.06	0.55	0.29	0.44	0.24
K_2O	16.47	15.23	15.51	14.20	17.60	16.55	18.70	17.35	19.63	17.84	19.81	18.14
MgO	0.11	0.24	0.23	0.48	0.01	0.03	0.01	0.03	0.02	0.05	0.02	0.04
MnO_2	0.45	0.45	0.22	0.21	0.01	0.01	0.01	0.01	0.02	0.02	0.03	0.03
Na_2O	0.32	0.45	0.76	1.05	0.07	0.10	0.07	0.10	0.06	0.08	0.05	0.07
NiO	0.02	0.02	0.06	0.07	0.00	0.00	0.00	0.00	0.00	0.00	0.00	0.00
P_2O_5	0.13	0.08	0.15	0.09	0.09	0.06	0.07	0.04	0.38	0.23	0.22	0.14
PbO	23.84	9.30	23.26	8.99	25.31	10.04	27.41	10.73	29.84	11.45	30.69	11.86
SrO	0.00	0.00	0.01	0.01	0.00	0.00	0.00	0.00	0.00	0.00	0.00	0.00
TiO_2	0.03	0.01	0.03	0.01	0.03	0.01	0.02	0.01	0.02	0.01	0.02	0.01
ZnO	0.03	0.04	0.01	0.01	0.00	0.00	0.01	0.01	0.00	0.00	0.00	0.00
	100	100	100	100	100	100	100	100	100	100	100	100

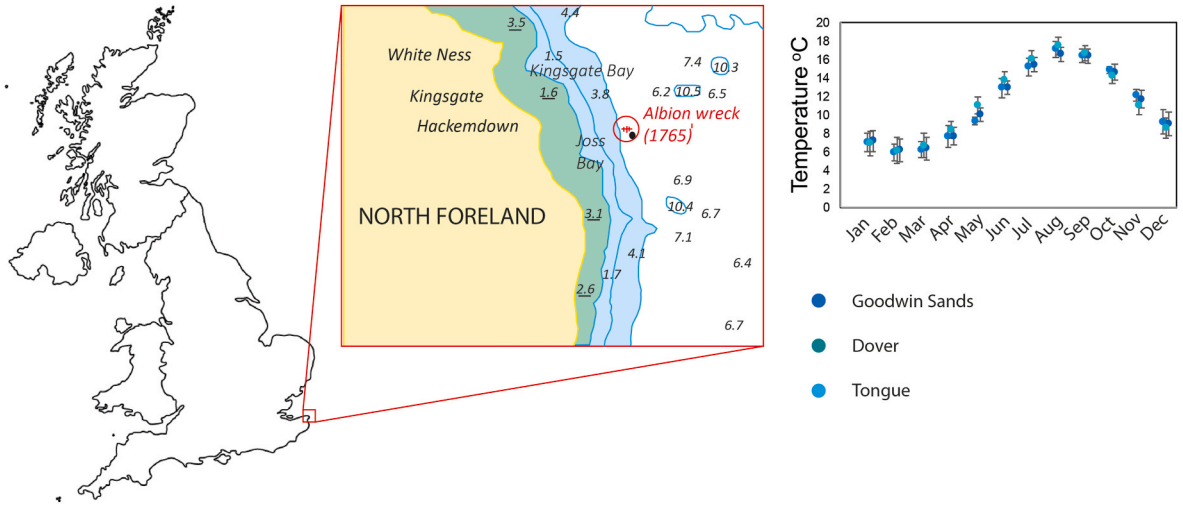

Fig. 3. left - location of the shipwreck Albion wreck site 51° 22.9' N 001° 27.2' E. Right - average temperature from three stations within 16 nautical miles of the Albion 1) Dark Blue = Goodwin Sands 51° 13.0' N 001° 36.0' E, Depth 3 m (average of 83 years between 1880 and 1985), 2) Green = Dover, 51° 07.0' N 001° 21.0' E (average of 53 years between 1926 and 1985), 3) Light Blue = Tongue 51° 30.6' N 1° 23.0' E (average of 10 years between 1975 and 1984). Data sourced from Morris et al. (2016). (For interpretation of the references to colour in this figure legend, the reader is referred to the Web version of this article.)

prevalent in areas likely to have experienced high stress, for example underneath biological growth or at sample corners and are likely the result of widening micro-cracks.

Alteration layers were intermittently observed on the exterior of the samples (e.g. Fig. 5C and D), presumably due to some having been detached during sample handling and storage, or possibly by *in-situ* abrasion, and were best preserved in cracks and crevices (e.g. Fig. 5A, B and 5F). Although the structure of alteration layers appeared different in confined cracks, when compared to those that formed freely on the surface of the glass, their chemistry was comparable.

Analysis of alteration layers from Glass 5 (green glass) by EDX and EPMA revealed two distinct chemical environments. The first environment was rich in silicon (14–15 atom %) and potassium (3–5 atom %), elements that were likely sourced primarily from within the glass but also containing magnesium (2.5 % atom %) and iron (22–28 % atom %) with minor aluminium (0.3–0.7 atom %) from the surrounding sediment and corroding wreck (Table 3; Figs. 6–8). The second chemical environment was composed of lead (8–23 atom %) from the glass and phosphorus (12–19 atom %), calcium (14–26 atom %), iron (6–10 atom %) and zinc (1–1.7 atom %) from the surrounding environment (plus minor sulphur, strontium, titanium and vanadium (<1 atom %)) (Table 3; Fig. 7).

3.1.4. Analysis of the iron rich phase

In the glass, Fe was present in very low quantities, 0.079 ± 0.016 atom % as measured by EPMA, and therefore to account for the presence of such extensive Fe-rich alteration there must have been sequestration not only of Fe released from the glass but also a contribution from the surrounding environment (either the seawater, iron bearing minerals in the sediment or materials likely associated with the corroding shipwreck). Seawater Fe concentrations are typically low (10–100 ppb; Armstrong, 1957), however concentrations could be higher in the vicinity of the corroding wreck that would have contained many iron fixtures and fittings. Iron-rich minerals including pyrite (FeS), iron-oxyhydroxides ($FeOH_2$) and iron-rich smectites have been observed previously in the alteration layers of corroded glass samples retrieved

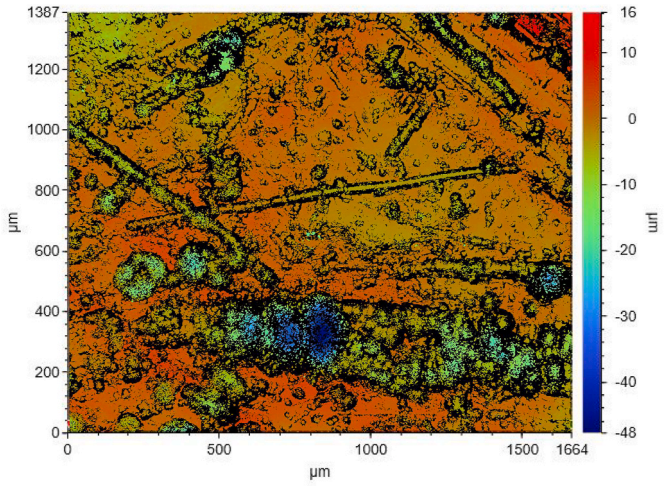

Fig. 4. Vertical scanning interferometry using visible light employed to image of preferential attack on the glass surface including pitting and corrosion along scratches. Approximately 20 images were taken in total and Vision software used to calculate the surface area and depth of features.

from shipwrecks (Table 4 and references therein).

On samples taken from Glass 5 (green glass), Fe K-edge XANES was used to probe the speciation and local coordination environment of Fe in the iron-rich zones. Zones were first located in cracks using microfocus XRF (SI Figs. 7, 8 and 9). The shape of the XANES spectra collected (Fig. 9A and B) showed no direct match to any standard measured although spectra have features in common with Fe-silicate phases augite, Fe-smectite bearing clay (boom clay; Frederickx et al., 2021), andradite and spectra reported in the literature for Fe-bearing glasses (Wilke et al., 2004; Farges et al., 2004; McKeown et al., 2024). Analysis of the pre-edge feature (indicated by the black dotted line) gave more information regarding the coordination number and valence state of Fe. The pre-edge centroid position depends strongly on the Fe oxidation state (Wilke et al., 2001, 2004), whereas the pre-edge area indicates the Fe coordination geometry (in the case of Fe this is usually 4, 5 or 6 fold). Low intensities refer to geometries with a centre of symmetry (e.g., octahedral) whilst high intensities are indicative of non-centrosymmetric geometries (e.g., tetrahedral) (Fig. 9). On a plot of the pre-edge intensity vs centroid position (Fig. 9C), samples grouped close to Fe^{3+} and $Fe^{2+}/^{3+}$ bearing silicate mineral standards but with peak intensity suggesting a less centrosymmetric coordination, likely indicative of a greater contribution from tetrahedral Fe (SI Table 2, SI Fig. 10; Fig. 9C). Comparing the fits of the pre-edge features with those of standards they are most similar to natural minerals of vesuvianite or augite which, although having theoretical 6-fold coordination, fit best with single peak indicative of a non-centrosymmetric structure (for example some Fe in 4 or 5-fold coordination (SI Fig. 10).

Geochemical modelling in PHREEQC suggests that phyllosilicates, oxides and hydroxides are all thermodynamically favourable under the pH and temperature conditions around the shipwreck (SI Tables 3 and 4). The observation of fibrous, needle-like crystals under SEM (Fig. 5C) could indicate silicates or hydroxides, however, the co-location of Fe and Si observed by EPMA (Figs. 5 and 7), evidence from Fe K-edge XANES, combined with the needle-like crystal form is consistent with Fe(III)-rich phyllosilicates such as the dioctahedral pyllosilicate nontronite $(Ca_{.5}(Si_7Al_{.8}Fe_{.2})(Fe_{3.5}Al_{.4}Mg_{.1})O_{20}(OH)_4)$ that can display a variety of morphologies including lath-shaped and fibre-like crystals (Fernández-Caliani et al., 2004; Cuadros et al., 2018). Nontronite is characterized by the presence of Fe^{2+} and Fe^{3+} in octahedral positions and minor Fe^{3+} in tetrahedral positions (arranged as an octahedral sheet sandwiched between two tetrahedral sheets with two thirds of the octahedral sites occupied by trivalent cations) (Gates et al., 2002; Palchik et al., 2013; Qian et al., 2023). In the majority of nontronite samples, Fe is predominantly (>95 %) in the octahedral (6 fold) coordination state, however, evidence presented by Gates et al. (2002) suggests that end members with a higher Fe content have a greater number of Si-tetrahedral sites occupied by Fe^{3+}. Gates et al., conclude that tetrahedral Fe^{3+} is likely to be present in samples containing >34 % wt % Fe_2O_3 and samples from this study Fe was measured as high as 28 atom % Fe (58 wt % Fe_2O_3). In the same area, Si was measured at 13 atom % (22 wt % SiO_2) with minor Mg (2.5 wt % MgO), K (6.5 wt % K_2O) and Ca (2.0 wt % CaO) all of which are elements associated with clay minerals and supporting the hypothesis that Fe-silicate phases or their poorly crystalline precursors are forming in these systems.

In the field, Verney-Carron et al. (2010) previously described cracks in the external zone of an altered Roman glass block filled with magnesium and iron-rich smectites that were brown in colour. Furthermore, poorly crystalline Fe and Mg rich smectites have been identified in laboratory experiments (e.g. Stroncik and Schmincke, 2001; Maeda et al., 2001; Crovisier et al., 2003; Thien et al., 2010; Parruzot et al., 2015; Arena et al., 2017; Carrière et al., 2019; Carriere et al., 2021; Corkhill et al., 2022) where glasses either contain Fe or have been in contact with Fe-containing media/minerals. No evidence for pyrite was observed in the glasses from the Albion (Fe was not co-located with S), unlike on soda-lime-silica and lead silicate glasses from the wrecks of the *Amsterdam* (sunk off Hastings in 1749) and the *Drottingin af Sverige* (sunk off Lerwick in 1745) both of which contained Fe-hydroxide and Fe-sulphate phases (pyrite) after alteration at ~10°C (Cox and Ford, 1989). Pyrite was also observed in altered glass from the *Iulia Felix* after exposure to seawater for 1800 years at 15 °C (Silvestri et al., 2005). The absence of pyrite is likely the result of the wreck's shallow location oxygenated by wave action but with the possibility of localised anoxic zones in cracks and crevices.

3.1.5. *Analysis of the lead rich phase*

The second alteration environment is dominated by Pb-rich phases contains both Ca and P. Whilst Pb-phosphate $(Pb_3(PO_4)_2$ and pyromorphite $(Pb_5(PO_4)_3OH))$ phases are both possible, chemical mapping and stoichiometric calculation suggests a mixed phase such a non-stoichiometric lead-substituted apatite (e.g. $(Pb,Fe,Zn)_2Ca_3(PO_4)_3(OH,F,Cl)$ (Table 5; Ellis et al., 2006). The calculated Pb/P ratio is lower than the 1.67 characteristic of pure Pb-apatite and implies a more disordered and likely amorphous structure. At the micron-scale resolution achievable by EMPA it appeared that significant Zn (1–2 atom %) and Fe (5–18 atom %) were co-located with Pb, Ca and P in this phase (Fig. 7). Mineral identification by raman spectroscopy was hampered by fluorescence such that peaks could not be reliably distinguished so µXANES was used to probe the P K-edge and Ca K-edge to determine local structure (Figs. 10 and 11).

Phosphorus K-edge XANES supports the conclusion of a mixed Pb,Ca - apatite phase with features similar to the chlorapatite and fluorapatite standards: no pre-edge feature (blue dashed line), the white line at 2152 eV (orange dashed line), a shoulder to the right of the white line at 2156 eV (green dashed line) and a post edge peaks at 2162 eV (red dashed line) and 2170 eV (Fig. 10; Franke and Hormes, 1995; Beauchemin et al., 2003; Ingall et al., 2011; Giguet-Covex et al., 2013).

XANES spectroscopy was also performed at the Ca–K edge (4037 eV) at 11 points around the same sample location on Glass 5 (green glass) on which previous Fe k-edge XANES and EPMA analysis was conducted (Fig. 10A) and were compared to known standards including carbonates, phosphates and silicates (Fig. 10). A key feature observable in standard spectra is a prominent pre-edge feature at 4039 eV (dark blue dashed line) that increases in intensity when the local symmetry around the calcium atom is distorted (Martin-Diaconescu et al., 2015). Centro-symmetric octahedral (6 fold) coordinated structures such as Ca $(OH)_2$ or calcite display a low intensity double peaked pre-edge feature (due to having little or no p−d mixing) whereas minerals in which Ca is present in seven and eight-fold coordination such as apatite, epidote and

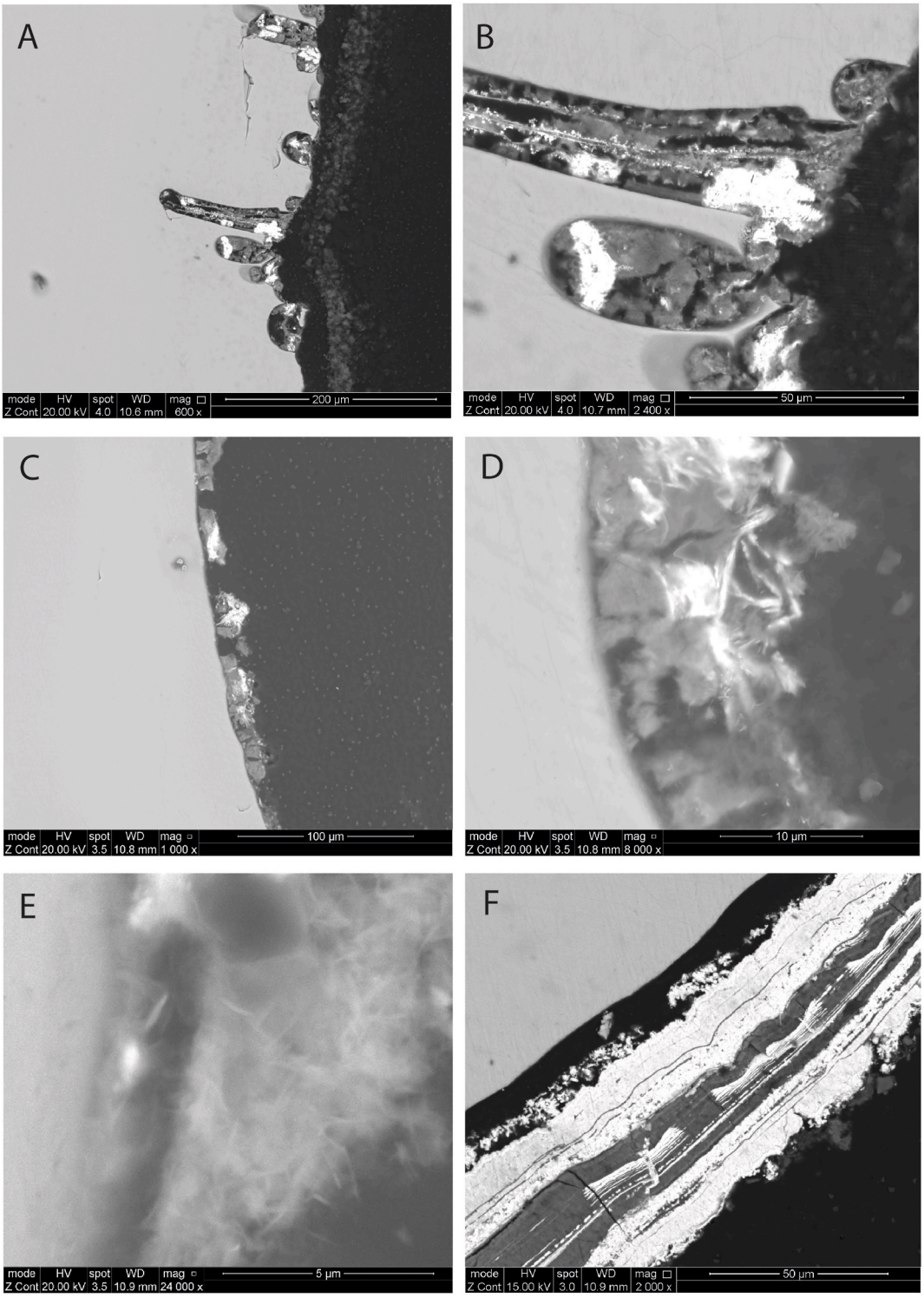

Fig. 5. SEM images of A & B, vermiform features containing alteration, C-E, alteration on the surface of glass ingots comprising bright phases rich in Pb and needle like crystals rich in Fe and F, alteration in a large crack.

ilvaite have distorted/broken centro-symmetry (where p−d mixing becomes favoured). This results in a single peak with increased intensity accompanied by a slight shift towards higher energies with increasing coordination number (Fig. 11B; SI Fig. 11; Sowrey et al., 2004). A single pre-edge peak is prominent in all sample spectra (Fig. 11C; SI Fig. 11) indicating a higher coordination number and ruling out six-fold coordinated structures such as calcium carbonate and calcium hydroxide in favour of calcium phosphates or silicate phases (SI Fig. 11). This is in agreement with the co-location of P and Pb with Ca and the fact that presence of P has been shown to inhibit the precipitation rates of carbonate minerals (e.g. aragonite and calcite) (Lin and Singer, 2006; Tadier et al., 2017). Ca XANES spectra for sample locations do not match the features of well crystalline apatite standards (both those measured in this study and those available in the literature) (Prietzel et al., 2021). The shoulder to the left of the main peak (white line) in position 4044 eV (purple dashed line) is absent in sample XANES except in positions 1, 2

Table 3
Elemental composition in atom % of the glass alteration layer in positions 1–8 (Fig. 8) compared to the unaltered glass matrix (average of five positions).

Element Atom %	Matrix	Fe rich	Fe rich	Pb rich	Pb rich	Pb rich	Pb rich	Pb rich	Pb rich
		1	2	3	4	5	6	7	8
Al	0.0 75 ± 0.021	0.745 ± 0.011	0.378 ± 0.009	0.025 ± 0.190	0.092 ± 0.017	0.055 ± 0.064	0.142 ± 0.015	0.221 ± 0.021	0.296 ± 0.022
O	60.17 ± 0.439	45.25 ± 0.389	51.98 ± 0.364	24.07 ± 0.628	34.47 ± 0.686	30.00 ± 0.693	46.496 ± 0.577	26.95 ± 0.695	28.511 ± 0.604
S	0.013 ± 0.009	0.444 ± 0.018	0.126 ± 0.010	0.833 ± 0.051	0.777 ± 0.039	0.804 ± 0.044	1.025 ± 0.034	1.323 ± 0.051	1.363 ± 0.055
K	6.945 ± 0.024	5.433 ± 0.026	3.523 ± 0.017	0.264 ± 0.011	0.278 ± 0.010	0.191 ± 0.009	0.309 ± 0.008	0.484 ± 0.013	0.288 ± 0.011
Ca	0.034 ± 0.004	1.399 ± 0.013	0.759 ± 0.008	14.89 ± 0.068	18.85 ± 0.068	20.17 ± 0.075	16.71 ± 0.052	19.393 ± 0.074	26.778 ± 0.088
Cl	0.027 ± 0.003	0.139 ± 0.005	0.033 ± 0.003	2.087 ± 0.030	2.945 ± 0.031	2.314 ± 0.029	1.367 ± 0.017	1.784 ± 0.026	1.557 ± 0.025
P	0.022 ± 0.006	0.492 ± 0.016	0.484 ± 0.013	19.422 ± 0.116	14.91 ± 0.122	18.123 ± 0.140	12.64 ± 0.088	12.569 ± 0.118	15.131 ± 0.136
Pb	3.984 ± 0.022	0.635 ± 0.012	0.537 ± 0.009	23.735 ± 0.116	11.43 ± 0.073	16.518 ± 0.093	10.309 ± 0.054	12.309 ± 0.079	8.689 ± 0.070
V	0.006 ± 0.005	0.015 ± 0.005	0.012 ± 0.004	0.144 ± 0.019	0.077 ± 0.015	0.056 ± 0.016	0.036 ± 0.009	0.036 ± 0.015	0.044 ± 0.014
Fe	0.079 ± 0.016	28.07 ± 0.121	22.60 ± 0.090	9.858 ± 0.132	10.08 ± 0.120	6.948 ± 0.112	5.834 ± 0.072	18.493 ± 0.157	11.05 ± 0.141
Cr	0.009 ± 0.009	0.024 ± 0.013	0.001 ± 0.010	0.014 ± 0.049	0	0	0.027 ± 0.027	0.026 ± 0.042	0.158 ± 0.048
Ti	0.013 ± 0.012	0.060 ± 0.015	0.062 ± 0.011	0.0020.048	0.100 ± 0.041	0.048 ± 0.044	0.052 ± 0.026	0.087 ± 0.040	0.051 ± 0.046
Co	0.01 ± 0.01	0.049 ± 0.028	0.019 ± 0.020	0.147 ± 0.107	0.083 ± 0.027	0.011 ± 0.095	0.061 ± 0.055	0.148 ± 0.084	0.030 ± 0.099
Mn	0.02 ± 0.01	0.033 ± 0.013	0.072 ± 0.010	0.048 ± 0.046	0.080 ± 0.037	0.095 ± 0.040	0.041 ± 0.025	0.044 ± 0.037	0.167 ± 0.040
Si	28.69 ± 0.07	13.91 ± 0.065	15.90 ± 0.057	0.852 ± 0.029	0.873 ± 0.027	0.642 ± 0.024	0.869 ± 0.020	1.363 ± 0.033	0.370 ± 0.020
Sr	0.00	0.004 ± 0.012	0.020 ± 0.011	0.070 ± 0.047	0.294 ± 0.049	0.154 ± 0.041	0.225 ± 0.027	0.285 ± 0.039	0.279 ± 0.036
Na	0.00	0.823 ± 0.022	0.850 ± 0.019	1.563 ± 0.052	2.208 ± 0.055	1.899 ± 0.050	1.953 ± 0.040	2.598 ± 0.058	2.561 ± 0.066
Mg	0.00	2.414 ± 0.019	2.511 ± 0.016	0.294 ± 0.024	0.712 ± 0.025	0.400 ± 0.022	0.809 ± 0.017	0.683 ± 0.024	0.892 ± 0.025
Zn	0.00	0.068 ± 0.396	0.129 ± 1.838	1.679 ± 69.16	1.723 ± 8.841	1.567 ± 22.18	1.088 ± 5.029	1.203 ± 6.495	1.786 ± 12.11
	100	**100**	**100**	**100**	**100**	**100**	**100**	**100**	**100**
Pb/P	–	**-**	**-**	**1.22**	**0.76**	**0.91**	**0.81**	**0.98**	**0.57**
Ca/P[a]	–	**-**	**-**	**0.76**	**1.26**	**1.11**	**1.32**	**1.54**	**1.77**
(Pb + Ca)/P	–	**-**	**-**	**2.03**	**2.03**	**2.02**	**2.13**	**2.45**	**2.34**

[a] the Ca/P ratio for stoichiometric apatite is 1.67.

and 3 that have a narrow white line more similar to the Ca-silicate standard epidote (Fig. 11C). A broadening of the white line (green dashed line), possibly encompassing a shoulder of near equal intensity, is visible in positions 4, 5,6,8,9,10 and the appearance of a feature around 4058 eV (light blue dashed line) are more similar to XANES standards for Chloro- and Fluorapatite. It is likely that the inclusion of so many additional elements including Si, Zn, Pb and Fe has resulted in a poorly crystalline or mixed phase assemblage.

Whilst seawater usually contains only trace quantities of dissolved phosphate, concentrations are likely to be elevated near to a source of organic matter (for example a corroding shipwreck). Phosphorus was previously observed by Silvestri et al. (2005) to accumulate along with Mn, Fe, and Ca near the surface of glass alteration layers in contact with marine sediment although no detail was given in this study regarding the mineral phases that formed. Calcium phosphate minerals have also been observed on glasses altered under atmospheric conditions that contained both Ca and P (e.g. Sessegolo et al., 2020; Verney-Carron et al., 2023) and glasses altered in terrestrial soils (e.g. Thorpe et al., 2024).

3.1.6. *Biological growth*

There has been recent renewed interest in the role of biological processes in glass alteration. A review article by Weaver et al. (2021) documented historical publications on the role of lichen and associated symbiotic bacteria in the degradation of church window glass, the development of anti-microbial glasses in the 1940's and microbial acceleration of mineral (including glass) weathering. More recently, research has shown evidence that pseudomonas bacteria are responsible for browning observed on medieval type glasses (Ferrand et al., 2015; Valbi et al., 2023; Boutillez et al., 2024), that microbes are stimulated by phosphorus containing glasses in laboratory systems (Thorpe et al., 2024) and that microorganisms can accelerate the weathering of basaltic glass (Perez et al., 2016). In a marine environment, glasses recovered from shipwrecks have been colonised by a variety of organisms including calcareous algae, marine worms, barnacles and bryozoan colonies (Silvestri et al., 2005; Cullimore and Johnston, 2008; Palomar and Llorente, 2016; Fears et al., 2019). Microbiological interactions with glasses retrieved from shipwrecks are impossible to determine as the samples are generally dried out and contaminated before they can be swabbed for microbial DNA, however, it recognised that a bacterial microbiome accompanies the settlement of larger organisms such as barnacles (Aldred and Nelson, 2019).

Calcareous deposits on the surface of glasses from the Albion were identified as barnacle baseplates likely resulting from the attachment and growth of common acorn barnacles (possibly *Balanus crenatus*) and in several cases by bryozoan colonies (possibly *Conopeum reticulum*) (SI Figs. 1–6). Considering their 220 years on the seabed these samples were sparsely colonised with the surface area covered (0–46 %; SI Table 5)

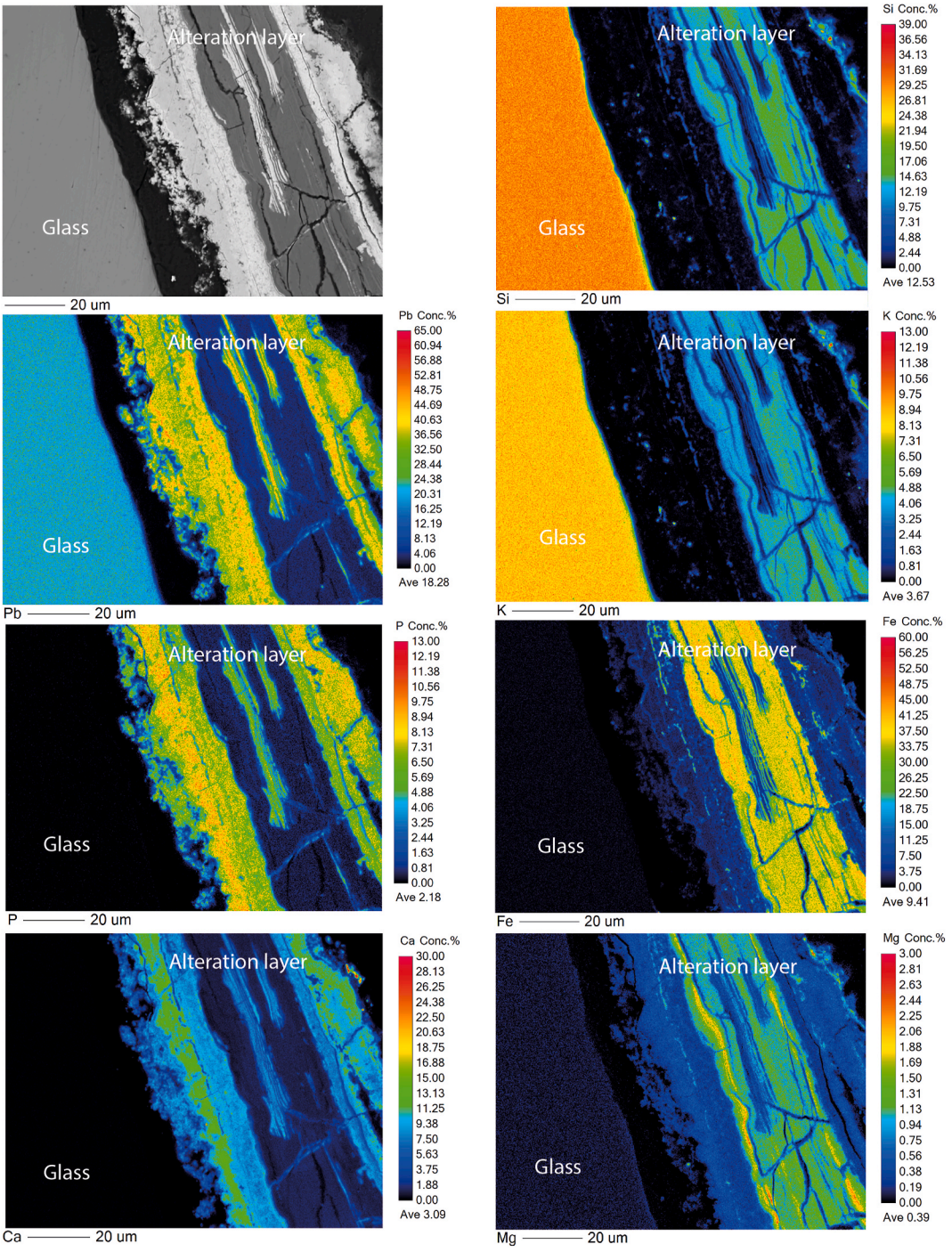

Fig. 6. Electron microprobe analysis of major elements (those present above 2 %) in Glass 5 (green glass) alteration layers. Si, Pb, K and minor Mg were sourced from the glass, whilst P, Fe, Ca and further Mg have sequestered from the environment. (For interpretation of the references to colour in this figure legend, the reader is referred to the Web version of this article.)

and with the highest number of barnacle base-plates observed on the plano-convex blue glass ingots. It was not clear whether this increase in colonisation was due to the blue glasses occupying a more exposed location (e.g. the top of the pile) or to reasons relating to their chemistry.

To test the impact of glass chemistry, laboratory settlement assays were performed to better understand the colonisation dynamics of the different glass compositions by a typical biofouling barnacle, *Amphibalanus improvisus* (SI Fig. 12). The overarching conclusion was that all glass surfaces, including a borosilicate control, reduced settlement of barnacle larvae compared to a positive laboratory standard, polystyrene, which was included in assays as an attractive settlement substrate for barnacles. The results for Glass 1 (blue glass), Glass 4 (clear glass), Glass 6 (green glass) were consistent across both replicate assays. For Glass 2 (blue glass), Glass 3 (clear glass) and Glass 5 (green glass), results differed between assays, however, due to the low larval settlement across all glasses, there was insufficient resolution to draw conclusions of significance (Fig. 12). Interestingly, although Glass 1 (blue) did not receive any settlement in either of the assays, Glass 3 (clear) and Glass 5 (green) also received zero settlement in assay two. Although all glasses contained multiple biotoxic elements that could deter the settlement and growth of marine organisms, including Pb, Cu, Ni and Co (SI Table 5), these results point to the Pb found within the composition of all of the

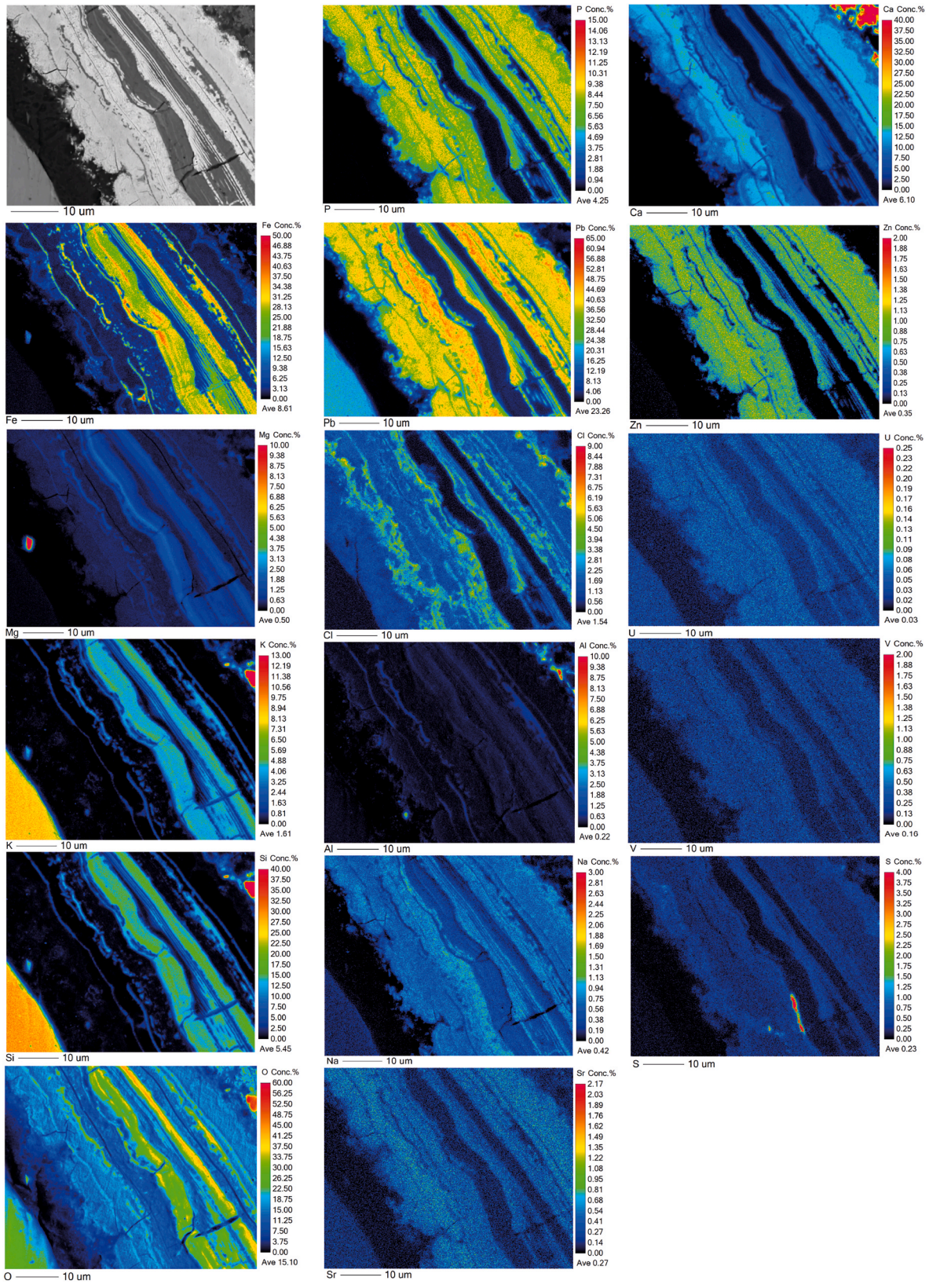

Fig. 7. EPMA analysis of major and minor elements identified in Glass 5 (green glass) alteration layers. (For interpretation of the references to colour in this figure legend, the reader is referred to the Web version of this article.)

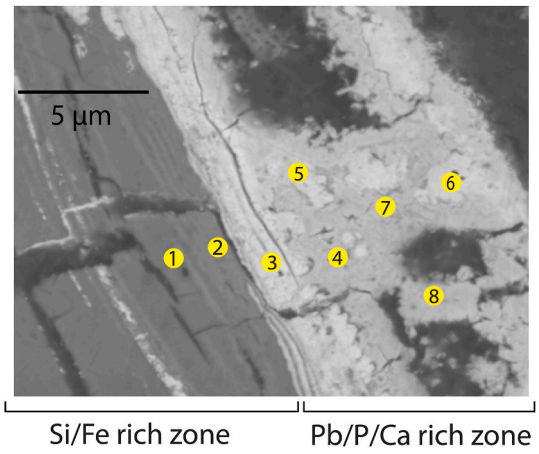

Fig. 8. SEM (backscatter detection mode) image of alteration layer zones and location of spot analysis on Glass 5 (green glass) described in Table 3. (For interpretation of the references to colour in this figure legend, the reader is referred to the Web version of this article.)

Table 4
Summary of secondary alteration minerals observed on shipwreck glasses exposed to natural marine conditions.

Reference "Ship"	Glass	Time exposed (Date sunk)	Alteration thickness	Alteration mineralogy
Cox and Ford (1989) "Amsterdam"	Alkali-calcium-silicate	~240 years (sunk 1749) (13 °C)	350–600 µm layers	$(Fe,Mg)OH_2$, $CaSO_4.2H_2O$ (gypsum) FeS (Pyrite)
Cox and Ford (1989) *"Drottengin af Sverige"*	Alkali–calcium-silicate & some K-lead silicate	~240 years (sunk 1745) (10 °C)	350–600 µm layers	$K_2Pb_2Si_2O_7$ FeS (Pyrite)
Silvestri et al., (2005) *"Iulia Felix"*	Soda-lime-silica	1800 years (14–15 °C)	10–100 µm gel + 200–1000 µm alteration	FeS (Pyrite) Fe rich zones towards the outside of the altered layer.
Verney-Carron et al. (2010), 2008	Soda-lime-silica	1800 ± 50 years (15 °C)	400–500 µm	MgFe-rich smectites, calcite, aragonite, hydrated Ca-silicate and zeolites
Anastassiades and Ellis (2008) *"Uluburun"*	Soda-lime-silica	3400 years	>1 cm	
Palomar 2018 "Navidad"	soda-lime-silica or mixed-alkali silicate glasses	>100 years (28 °C)	Not reported	Precipitates high in MnO, Fe_2O_3 and PbO.

glasses, and would align with the known potency of lead as a biocidal agent and its historic use in antifouling coatings for that purpose (e.g. Aldred and Clare, 2008).

Where barnacle settlement was successful on naturally altered samples, the contact was clean and free of alteration (Fig. 13D). To attach to a surface, barnacles lay down a protein based polymerized cement layer (Dickinson et al., 2009; Aldred et al., 2020) that can be corrosive as it contains both surfactants (to clear organic matter from the substrate) and strong oxidases. Once set, this layer is insoluble under most natural conditions and thus shields the glass surface from further contact with water (Kamino, 2013; Dickinson et al., 2009). Despite this, it is possible that barnacles can harbour bacteria beneath their base plates that have been shown to contribute to microbially induced corrosion (for example of metal surfaces). It is possible that metal reducing bacteria may affect glass in a similar way, however no evidence of pitting under or around barnacle base plates was seen in this study. Similarly, Palomar (2018) notes the growth of bryozoans and barnacles on shipwreck glass surfaces but concludes that their presence was protective, shielding the glass from chemical attack, and that neither species attacks the glass directly. Bryozoan colonies, either preferentially attach to a rough surface or their growth has exerted stress on the glass surface and increased the prevalence of cracking and vermiform features under the colony (Fig. 13).

3.1.7. Laboratory tests

Laboratory tests were conducted using coupons cut from the centre of the original glasses, thus ensuring that the composition of samples was compositionally comparable to those of the naturally altered glasses (SI Fig. 13). Synthetic seawater was created using the recipe described in Table 2.

Initial powder dissolution tests, conducted in line with ASTM C1285 (the modified PCT-B test), confirmed that all glasses dissolved at a comparable rate when exposed to Type 1 water despite minor differences in their chemical composition (most notably the absence of Al_2O_3 from the green glass (Glasses 5 and 6)) (Fig. 14). In these high SA/V ration powder tests, the pH of the solution remained around neutral in all systems over the 28-day period. None of the shipwreck glass composition contained a suitable tracer element by which to track the dissolution rate of the glass dissolution. Typically, B or Li, are used as tracers as they are not retained in secondary alteration layer minerals. A commonly used alternative, Na, was only present in very low concentrations and, therefore, an accurate measurement of glass dissolution rates was not possible. An approximate normalised rate of 2.0 (±0.3) x 10^{-2} g m^{-2} d^{-1} was estimated from the release of K, that is only weakly retained in alteration minerals. K release was linear over the 28 days for the clear glass whilst a slight drop was observed after 28 days for both the blue and green glasses. The NL_i of Si and Pb was lower than that of K indicative of their greater retention in glass alteration layers (Fig. 14).

Monolith tests were then established for 12 months at 90 °C in synthetic seawater at a SA/V ratio of (~10 m^{-1}) and (0.4 m^{-1}) in order to grow a measurable alteration layer from which the chemistry and morphology could be determined and compared to alteration occurring evolved in a complex natural environment (SI Fig. 13). The lower SA/V experiments were conducted to ensure that elements in solution did not become depleted during the course of the experiment due to sequestration into glass alteration layers and that the buffering capacity of a larger solution volume maintained a pH closer to that of natural seawater (pH 8.5). Solution chemistry was monitored over four timepoints with pH data available for 58, 112, 262, and 365 days (Fig. 15) and elemental data for 112, 262 and 365 days (day 58 data was omitted as if failed to pass quality checks) (SI Figs. 14 and 15). As K is a major constituent of seawater, it was not possible to measure an alteration rate in these systems as the NL_K was within the error of triplicate ICP measurements (SI Figs. 14 and 15). Alteration layer thickness gives some indication of rate but a 1:1 relationship of volume of glass dissolved to volume alteration layer precipitated cannot be assumed due to the potential for differences in density and inclusion of elements sourced from the surrounding seawater. The thickness of alteration on samples altered at 90 °C in synthetic seawater under a SA/V 10 m^{-1} for 1 year was ~50 µm and ~60 µm where the SA/V was 0.4 m^{-1}. This was thicker or comparable to alteration layers found on natural samples which were between 10 and 15 µm on exterior surfaces and up to 50 µm within cracks. A year under accelerated conditions altered glass coupons to a similar, likely greater, extent than the same glasses were altered under marine conditions for 220 years at 6–18 °C. This is in-keeping with laboratory studies of temperature dependence for silicate and borosilicate glasses that report rates 2 orders of magnitude higher for nuclear waste glass compositions altered at 20 °C compared to 90 °C (Neeway

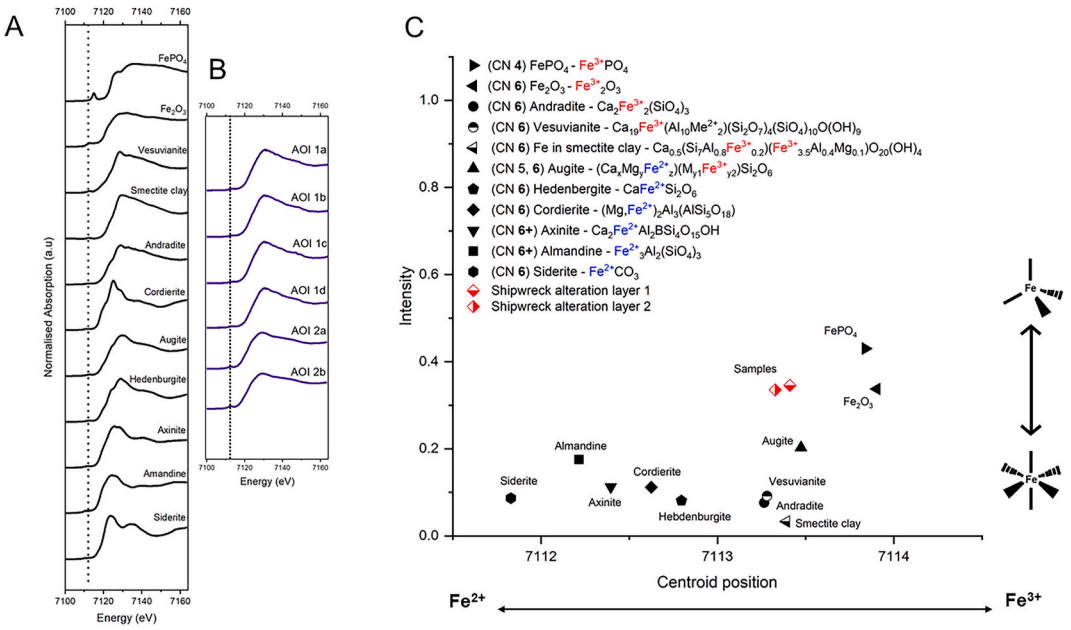

Fig. 9. A) Fe K-edge XANES spectra of Fe-bearing mineral phases, B) Fe K-edge XANES spectra of Fe rich alteration layers from Glass 5 (green glass) and C) plot of centroid position against peak intensity for standard Fe-bearing minerals and for samples taken from the iron and silica rich layer of Glass 5 (green glass). (For interpretation of the references to colour in this figure legend, the reader is referred to the Web version of this article.)

Table 5
Selected results from modelling in PHREEQC-3.7.0 (Minteq database) for identical seawater solutions with glass derived elements (SI Table 3) under natural conditions of pH 8.3 and 15 °C and laboratory conditions at 90 °C where the pH dropped to 6.5.

Phase	Formula	Saturation Index Natural system (pH 8.3, 15°C)	Saturation Index Laboratory system (pH 6.5, 90°C)
Ca-Nontronite	$Fe_2Al_{.33}Si_{3.67}O_{10}(OH)_2Ca_{0.165}$	27.63	19.12
K-Nontronite	$Fe_2Al_{.33}Si_{3.67}O_{10}(OH)_2K_{0.33}$	21.89	13.38
Mg-Nontronite	$Fe_2Al_{.33}Si_{3.67}O_{10}(OH)_2Mg_{0.165}$	27.44	18.93
Montmorillonite	$Mg_{0.485}Fe_{.22}Al_{1.71}Si_{3.81}O_{10}(OH)_2$	11.68	0.8
Muscovite	$KAl_3Si_3O_{10}(OH)_2$	15.45	8.26
Na-Nontronite	$Fe_2Al_{.33}Si_{3.67}O_{10}(OH)_2Na_{0.33}$	21.44	12.93
Kaolinite	$Al_2Si_2O_5(OH)_4$	9.33	5.23
Leonhardite	$Ca_2Al_4Si_8O_{24}$:$7H_2O$	26.39	12.37
Cerussite	$PbCO_3$	2.45	0.23
ClPyromorphite	$Pb_5(PO_4)_3Cl$	23.96	16.25
Hxypyromorphite	$Pb_5(PO_4)_3OH$	11.27	1.59
Hydcerussite	$Pb(OH)_2$:$2PbCO_3$	7.08	0.46
Hydroxyapatite	$Ca_5(PO_4)_3OH$	8.58	−3.02
Laumontite	$CaAl_2Si_4O_{12}$:$4H_2O$	6.78	0.99
Laurionite	PbOHCl	1.66	−0.07
Fe(OH)2.7Cl0.3	$Fe(OH)_{2.7}Cl_{0.3}$	7.76	5.2
Lepidocrocite	FeOOH	6.04	2.89
Mg-Ferrite	$MgFe_2O_4$	11.44	11.51
CuprousFerrite	$CuFeO_2$	13.25	8.8
Hematite	Fe_2O_3	18.05	16.59

et al., 2018).

In all systems containing clear or green glass, dissolution caused a reduction in pH to between pH 6.5–7.0 while seawater-only controls remained at pH of 8.5 throughout the 365-day test (Fig. 15). This decrease in pH could be caused by the precipitation of hydroxide containing secondary mineral phases that are thermodynamically favourable to form (SI Table 4; Table 5). Interestingly, the blue glass at lower SA/V does not display a decrease in pH. This could be because the Na content in these glasses is an order of magnitude higher than the clear and green glasses meaning that the decrease in pH is countered by ion exchange of H_3O^+ with Na.

This difference in pH between closed laboratory systems and open naturally buffered systems will have several important effects. Firstly, lower pH will affect the mechanism of glass dissolution through greater inter-diffusion of alkali elements with H_3O^+ at lower pH values. Secondly, pH will affect the saturation index of key secondary mineral phases that may precipitate in the alteration layer. PHREEQC modelling was used to predict the saturation indices of key secondary mineral phases in seawater condition (15 °C, pH 8.5) and laboratory conditions (90 °C, pH 6.5) demonstrating that the precipitation of most mineral phases is more thermodynamically favourable in the natural system at lower temperatures and higher pH. Regardless of which phases are

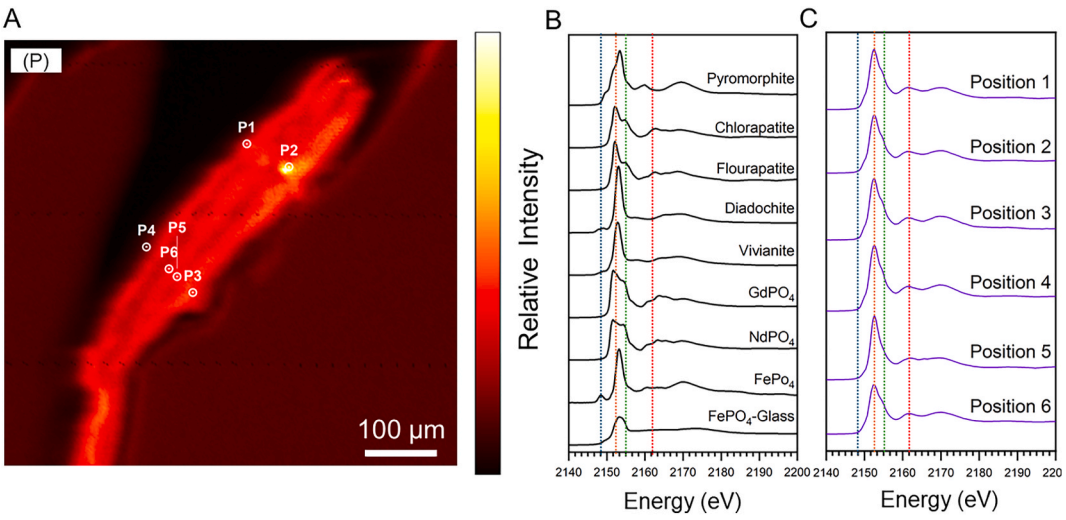

Fig. 10. A) Location of P K-edge XANES spot analysis on µXRF map of P. B) P K-edge XANES spectra of P-bearing minerals and C) P K-edge XANES spectra of spots 1–7 on alteration layers from Glass 5 (green glass). (For interpretation of the references to colour in this figure legend, the reader is referred to the Web version of this article.)

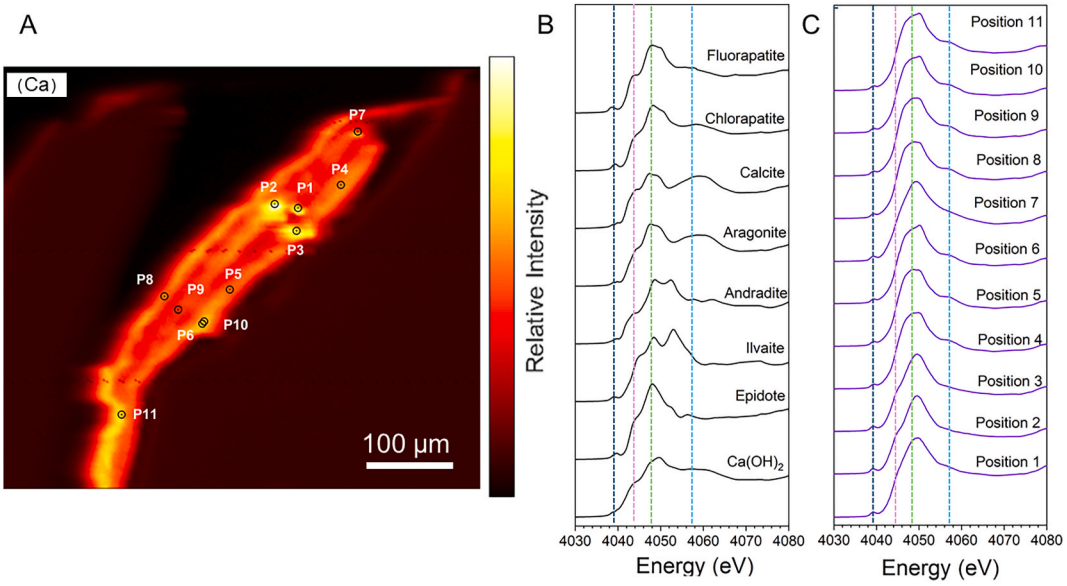

Fig. 11. A) Location of Ca K-edge XANES spot analysis on µXRF map of Ca. B) Ca K-edge XANES spectra of Ca-bearing mineral phases and C) Ca K-edge XANES spectra of Ca rich spots on alteration layers from Glass 5 (green glass). (For interpretation of the references to colour in this figure legend, the reader is referred to the Web version of this article.)

predicted to be thermodynamically favourable, the observed phase assemblage is dependent on kinetic factors and availability of elements in the system.

The alteration layer chemistry of 365 day samples was analysed by SEM-EDX and found to be similar for all glasses (SI Figs. 16–18). As with natural samples, the laboratory altered Glass 5 (green glass) was further analysed by EPMA (Fig. 16).

The alteration layer chemistry was found to be significantly different than those observed in naturally altered samples. The silica rich regions are rich in Mg with only minor Cu and Fe sourced from the glass. PHREEQC modelling predicts super saturation with regard to Mg-clay minerals (Mg-nontronite ($Fe_2Al_{.33}Si_{3.67}O_{10}(OH)_2Mg_{0.165}$), montmorillonite ($Mg_{0.485}Fe_{.22}Al_{1.71}Si_{3.81}O_{10}(OH)_2$) and sepiolite ($Mg_2Si_3O_{7.5}OH{:}3H_2O$)) Talc ($Mg_3Si_4O_{10}(OH)_2$) and Tremolite ($Ca_2Mg_5Si_8O_{22}(OH)_2$) (SI Table 4; Table 5). In this closed system the limited availability of Fe prevented its accumulation and the precipitation of the more thermodynamically favourable nontronite phase.

Instead of forming a Pb substituted-apatite phase, as found in natural samples, Pb in laboratory experiments associated with S and Cl indicative of lead sulphate or chloride phases like Lanarkite ($PbO{:}PbSO_4$), Laurionite (PbOHCl) and/or $Pb_2(OH)_3Cl$ all of which are predicted to be saturated or close to saturated in PHREEQC modelling (Fig. 16; SI Figs. 16–18; Table 5; SI Tables 3 and 4). What little PO_4^{3-} was present in solution, or as trace P_2O_5 from the glass, has also co-located with the Pb suggesting that Pb-phosphate would likely have been a dominant phase if the system was not limited with regard to P.

Differences in the chemistry and mineralogy of the Pb rich zone can be accounted for by the fact that natural samples had a continuous supply of PO_4^{3-} from an open system, likely augmented by nearby biological processes occurring as the wreck corroded. PHREEQC modelling of the natural system confirmed that lead phosphate phases (e.g.

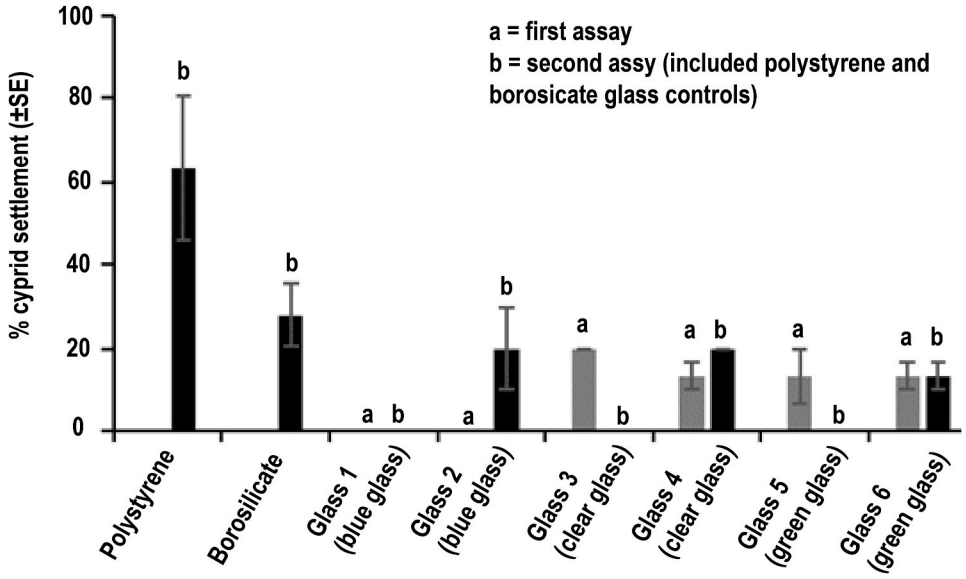

Fig. 12. The results of a laboratory settlement assay using three-day-old cypris larvae of the barnacle *Amphibalanus improvisus*. Average settlement after 48 h ± standard error.

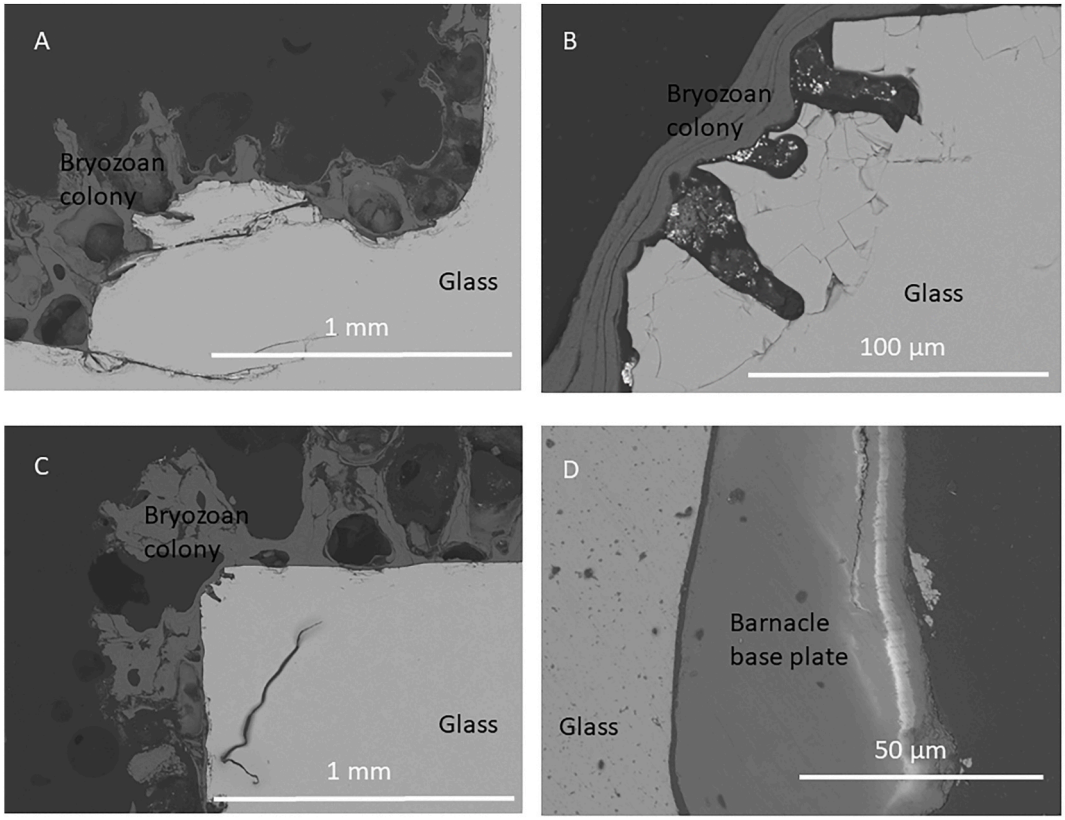

Fig. 13. SEM images (in backscatter detection mode). A, B and C show cracking and pitting of the glass under the bryozoan colony whilst D shows the clean adherence of a barnacle baseplate to the surface of the glass providing some protection from corrosion.

Pyromorphite ($Pb_5(PO_4)_3Cl$) $Pb_3(PO_4)_2$ and Pb substituted hydroxyapatite) are more thermodynamically favourable than lead sulphates and lead hydroxides under ambient seawater conditions. In closed system laboratory tests the PO_4^{3-} was a minor component (Table 1) quickly reacted leaving the remainder of the Pb to for a less thermodynamically favourable phases, however, in an open system such as the sea a large reservoir allows slow accumulation of PO_4^{3-} over time resulting in high concentrations in naturally altered samples. Similarly, a constant supply of Fe in the open seawater system (possibly only at ppb concentrations) has augmented Fe sourced from the glass and cause the element to accumulate over time causing Fe-silicate phases in place of Mg-silicate phases.

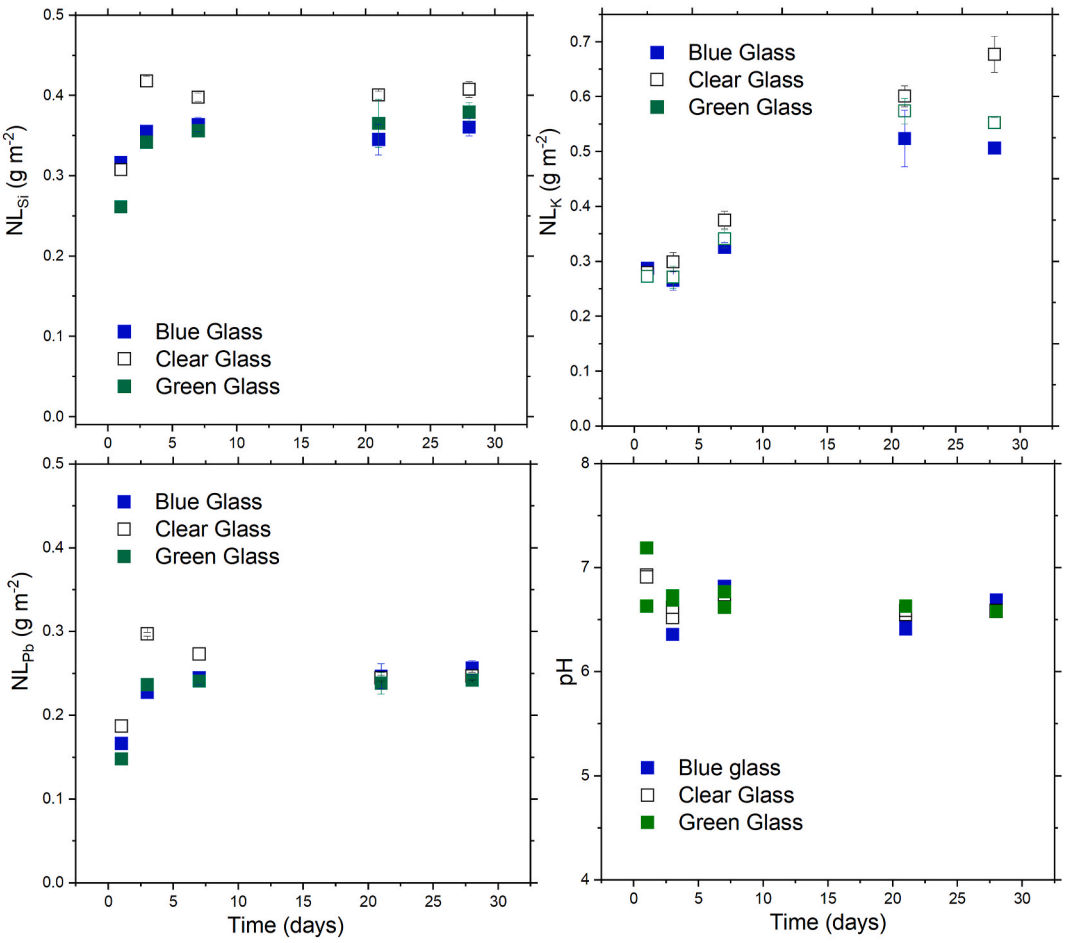

Fig. 14. Normalised mass loss (g/m^2) for K, Si and Pb for 28-day powder dissolution tests in DI water. Results are the average of triplicate analysis. Ph readings were taken at room temperature after the solution was allowed to cool.

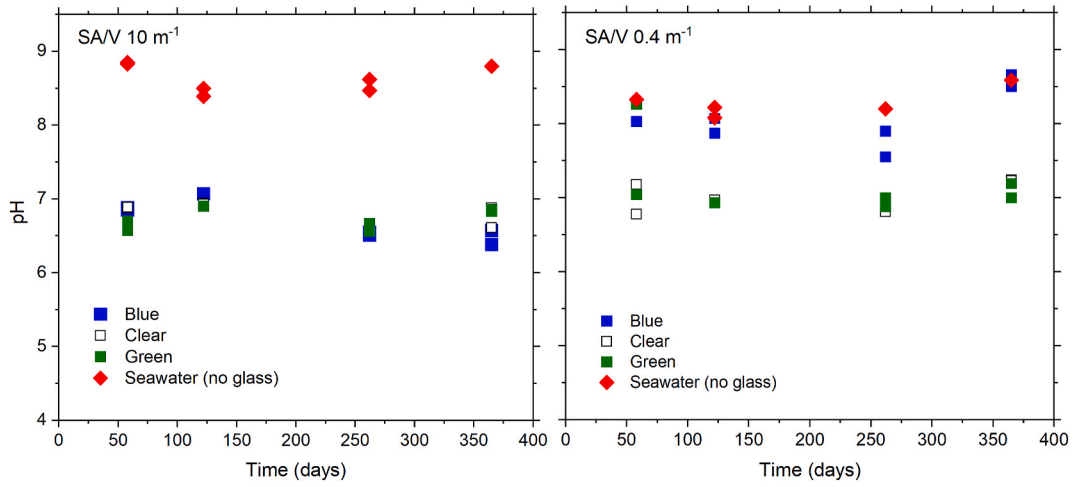

Fig. 15. PH in long term monolith dissolution tests with two different SA/V ratios (right) SA/V 10 m^{-1} and (left) SA/V 0.4. All pH readings were taken at room temperature after solution was allowed to cool.

4. Conclusion

Laboratory tests in synthetic seawater and closed systems, performed at elevated temperatures, failed to simulate the morphology or chemistry of alteration layers formed in a natural, open system. Results highlight the importance of minor elements, that can accumulate over long periods of time when glass is altering slowly. Results also point to the indirect effect of biological/microbiological processes in controlling the local geochemistry, for example in Fe and P cycling in the vicinity of the wreck. This study cautions against over-simplification of laboratory tests when attempting to estimate the long-term behaviour of materials in complex natural environments. It is important not to discount

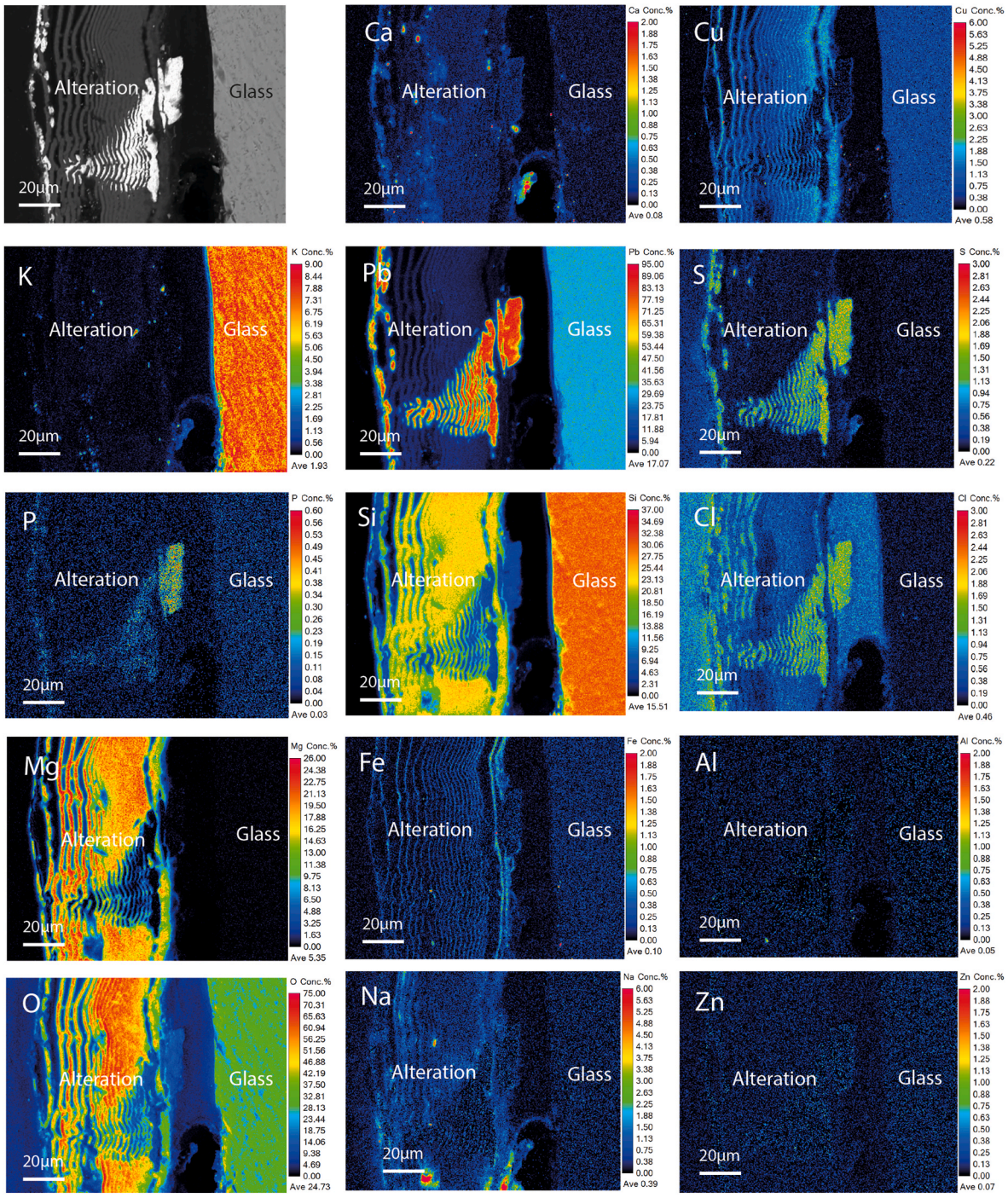

Fig. 16. EPMA analysis of major and minor elements identified after alteration of Glass 5 (green glass) for one year in synthetic seawater. (For interpretation of the references to colour in this figure legend, the reader is referred to the Web version of this article.)

elements present at low concentrations that may be constantly replenished from the surroundings.

If disposed of in the subsurface, glasses containing radioactive waste will alter in the presence of both natural (groundwater, natural rock forming minerals) and anthropogenic (steels, cements) materials. This study demonstrates that cumulative effects (e.g. slow sequestration of elements from surrounding rock or from the corroding steel canister) could be the controlling factor in determining secondary alteration phases and therefore the fate of radionuclides released from the glass. Both clay minerals and phosphates are able to sorb/sequester heavy metals and radionuclides and so their formation would beneficial to the safety case for radioactive waste disposal.

CRediT authorship contribution statement

Clare L. Thorpe: Writing – review & editing, Writing – original draft, Investigation, Funding acquisition, Formal analysis, Data curation, Conceptualization. **Nick Aldred:** Writing – review & editing, Formal analysis, Data curation. **Stuart Creasey-Gray:** Writing – review & editing, Data curation. **Martin C. Stennett:** Data curation, Formal analysis. **Eperke A. Rencz:** Data curation, Writing – review & editing. **Susan Nehzati:** Data curation. **Latham T. Haigh:** Data curation, Formal analysis, Writing – review & editing. **Garry Manifold:** Writing – review & editing, Formal analysis, Data curation. **Nishta Vallo:** Data curation. **Christoph Lenting:** Data curation. **Claire L. Corkhill:** Data curation.

Russell J. Hand: Writing – review & editing.

Declaration of competing interest

The authors declare that they have no known competing financial interests or personal relationships that could have appeared to influence the work reported in this paper.

Acknowledgements

The authors would like to acknowledge Colin Brain for the kind donation of all samples used in this study. CLT acknowledges the UK Engineering and Physical Sciences Research Council (EPSRC) for the award of a David Clarke Fellowship (EP/S012400/1), the Royal Society of Chemistry for the award of a Research Fund and the Royal Society for the award of a Dorothy Hodgkin Fellowship. GM would like to acknowledge funding from the UK Governments Nuclear Waste Services. CLC acknowledges EPSRC for the award of an Early Career Research Fellowship (EP/N017374/1). This research utilised the HADES/MIDAS facility at the University of Sheffield established with financial support from EPSRC under grant EP/T011424/1. Imaging was conducted at the Sorby Centre for Microscopy, with EPMA funded by the Royce Discovery Centre at University of Sheffield. Microfocus spectroscopy was conducted at the UK Diamond Light Source (I18) beamtime SP38045-1 and NSLS-II (B4).

Appendix A. Supplementary data

Supplementary data to this article can be found online at https://doi.org/10.1016/j.apgeochem.2025.106363.

Data availability

Data will be made available on request.

References

Aldred, N., Chan, V.B.S., Emami, K., Okano, K., Clare, A.S., Mount, A.S., 2020. Chitin is a functional component of the larval adhesive of barnacles. Commun. Biol. 3 (1), 31.
Aldred, N., Nelson, A., 2019. Microbiome acquisition during larval settlement of the barnacle *Semibalanus balanoides*. Biol. Lett. 15 (6), 20180763.
Aldred, N., Clare, A.S., 2008. The adhesive strategies of cyprids and development of barnacle-resistant marine coatings. Biofouling 24 (5), 351–363.
Allison, J.D., Brown, D.S., Novo-Gradac, K.J., 1991. MINTEQA2/PRODEFA2, a geochemical assessment model for environmental systems: version 3.0 user's manual. In: Environmental Research Laboratory, Office of Research and Development. US Environmental Protection Agency.
Anastassiades, A., Ellis, L., 2008. The conservation of glass ingots from the Bronze Age Uluburun shipwreck. Stud. Conserv. 53, 225–237.
Arena, H., Rébiscoul, D., Podor, R., Garcès, E., Cabie, M., Mestre, J.P., Godon, N., 2018. Impact of Fe, Mg and Ca elements on glass alteration: interconnected processes. Geochem. Cosmochim. Acta 239, 420–445.
Arena, H., Godon, N., Rébiscoul, D., Frugier, P., Podor, R., Garcès, E., Cabie, M., Mestre, J.P., 2017. Impact of iron and magnesium on glass alteration: characterization of the secondary phases and determination of their solubility constants. Appl. Geochem. 82, 119–133.
Arena, H., Godon, N., Rébiscoul, D., Podor, R., Garcès, E., Cabie, M., Mestre, J.P., 2016. Impact of Zn, Mg, Ni and Co elements on glass alteration: additive effects. J. Nucl. Mater. 470, 55–67.
Armstrong, F.A.J., 1957. The iron content of seawater. J. Mar. Biol. Assoc. U. K. 36, 509–517.
ASTM, 2021a. ASTM C1308-21: Standard Test Method for Accelerated Leach Test for Measuring Contaminant Releases from Solidified Waste.
ASTM, 2021b. ASTM C1220-21: Standard Test Method for Static Leaching of Monolithic Waste Forms for Disposal of Radioactive Waste.
ASTM, 2021c. ASTM C1285: standard test methods for determining chemical durability of nuclear. In: Hazardous, and Mixed Waste Glasses and Multiphase Glass Ceramics: the Product Consistency Test (PCT).
Beauchemin, S., Hesterberg, D., Chou, J., Beauchemin, M., Simard, R.R., Sayers, D.E., 2003. Speciation of phosphorus in phosphorus-enriched agricultural soils using X-ray absorption near-edge structure spectroscopy and chemical fractionation. J. Environ. Qual. 32 (5), 1809–1819.
Benedetti, D., Bontempi, E., Bertoncello, R., Dal Bianco, B., Pantos, E., Depero, L.E., 2007. Study of sea water influence on chemical and physical degradation of Roman glass. Il nuovo cimento della societa italiana di fisica. C, Geophyics and space physics 30, 27–33.
Boutillez, C., Perez, A., Verney-Carron, A., Guyot, F., Rossano, S., 2024. The role of Fe in the browning of medieval model glasses in the presence of the Pseudomonas putida bacteria strain. Int. Biodeterior. Biodegrad. 188, 105734.
Carmona, N., Garcia-Heras, M., Gil, C., Villegas, M.A., 2005. Chemical degradation of glasses under simulated marine medium. Mater. Chem. Phys. 94 (1), 92–102.
Carriere, C., Dillmann, P., Gin, S., Neff, D., Gentaz, L., Bruguier, F., Monnet, I., Gardes, E., Saheb, M., Foy, E., Nuns, N., 2021. The fate of Si and Fe while nuclear glass alters with steel and clay. npj Mater. Degrad. 5 (1), 16.
Carrière, C., Dillmann, P., Foy, E., Neff, D., Dynes, J.J., Linard, Y., Michau, N., Martin, C., 2019. Use of nanoprobes to identify iron-silicates in a glass/iron/argillite system in deep geological disposal. Corros. Sci. 158, 108104.
Corkhill, C.L., Mann, C., Eskelsen, J.R., Leonard, D.N., Mottram, L.M., Stennett, M.C., Ayling, J.M., Thorpe, C.L., Cole, M.R., Nicholas, S., Tappero, R., 2022. Surface interfacial analysis of simulant high level nuclear waste glass dissolved in synthetic cement solutions. npj Mater. Degrad. 6 (1), 67.
Cox, G.A., Ford, R.A., 1989. The corrosion of glass on the sea bed. J. Mater. Sci. 24, 3146–3153. https://doi.org/10.1007/bf01139033.
Crovisier, J.L., Advocat, T., Dussossoy, J.L., 2003. Nature and role of natural alteration gels formed on the surface of ancient volcanic glasses (Natural analogs of waste containment glasses). J. Nucl. Mater. 321 (1), 91–109.
Cuadros, J., Šegvić, B., Dekov, V., Michalski, J.R., Bardají, D.B., 2018. Electron microscopy investigation of the genetic link between Fe oxides/oxyhydroxides and nontronite in submarine hydrothermal fields. Mar. Geol. 395, 247–259.
Cullimore, D.R., Johnston, L.A., 2008. Microbiology of concretions, sediments and mechanisms influencing the preservation of submerged archaeological artifacts. Int. J. Hist. Archaeol. 12, 120e132.
Dal Bianco, B., Bertoncello, R., Milanese, L., Barison, S., 2004. Glasses on the seabed: surface study of chemical corrosion in sunken Roman glasses. J. Non-Cryst. Solids 343, 91.
Dickinson, G.H., Vega, I.E., Wahl, K.J., Orihuela, B., Beyley, V., Rodriguez, E.N., Everett, R.K., Bonaventura, J., Rittschof, D., 2009. Barnacle cement: a polymerization model based on evolutionary concepts. J. Exp. Biol. 212 (21), 3499–3510.
Ellis, D.E., Terra, J., Warschkow, O., Jiang, M., González, G.B., Okasinski, J.S., Bedzyk, M.J., Rossi, A.M., Eon, J.G., 2006. A theoretical and experimental study of lead substitution in calcium hydroxyapatite. Phys. Chem. Chem. Phys. 8 (8), 967–976.
EPA, 2021. The Geochemistry of the Waste Isolation Pilot Plant. Environmental Protection Agency report. EPA-402/R-21/002. Available at: https://www.epa.gov/system/files/documents/2022-02/the-geochemistry-of-the-waste-isolation-pilot-plant_final.pdf.
Farges, F., Lefrère, Y., Rossano, S., Berthereau, A., Calas, G., Brown Jr., G.E., 2004. The effect of redox state on the local structural environment of iron in silicate glasses: a combined XAFS spectroscopy, molecular dynamics, and bond valence study. J. Non-Cryst. Solids 344 (3), 176–188.
Farges, F., Rossano, S., Lefrere, Y., Wilke, M., Brown, G.E., 2005. Iron in silicate glasses: a systematic analysis of pre-edge, XANES and EXAFS features. Phys. Scripta 2005 (T115), 957.
Fears, K.P., Barnikel, A., Wassick, A., Ryou, H., Schultzhaus, J.N., Orihuela, B., Scancella, J.M., So, C.R., Hunsucker, K.Z., Leary, D.H., Swain, G., 2019. Adhesion of acorn barnacles on surface-active borate glasses. Phil. Trans. Roy. Soc. B 374 (1784), 20190203.
Fernández-Caliani, J.C., Crespo, E., Rodas, M., Barrenechea, J.F., Luque, F.J., 2004. Formation of nontronite from oxidative dissolution of pyrite disseminated in Precambrian felsic metavolcanics of the Southern Iberian Massif (Spain). Clays Clay Miner. 52 (1), 106–114.
Ferrand, J., Rossano, S., Loisel, C., Trcera, N., van Hullebusch, E.D., Bousta, F., Pallot-Frossard, I., 2015. Browning phenomenon of medieval stained glass windows. Anal. Chem. 87 (7), 3662–3669.
Franke, R., Hormes, J., 1995. The P K-near edge absorption spectra of phosphates. Phys. B Condens. Matter 216 (1–2), 85–95.
Frederickx, L., Honty, M., De Craen, M., Elsen, J., 2021. Evaluating the quantification of the clay mineralogy of the Rupelian Boom Clay in Belgium by a detailed study of size fractions. Appl. Clay Sci. 201, 105954.
Frugier, P., Minet, Y., Rajmohan, N., Godon, N., Gin, S., 2018. Modeling glass corrosion with GRAAL. npj Mater. Degrad. 2 (1), 35.
Gates, W.P., Slade, P.G., Manceau, A., Lanson, B., 2002. Site occupancies by iron in nontronites. Clays Clay Miner. 50 (2), 223–239.
Giguet-Covex, C., Poulenard, J., Chalmin, E., Arnaud, F., Rivard, C., Jenny, J.P., Dorioz, J.M., 2013. XANES spectroscopy as a tool to trace phosphorus transformation during soil genesis and mountain ecosystem development from lake sediments. Geochem. Cosmochim. Acta 118, 129–147.
Gin, S., Delaye, J.M., Angeli, F., Schuller, S., 2021. Aqueous alteration of silicate glass: state of knowledge and perspectives. npj Mater. Degrad. 5 (1), 42.
Ingall, E.D., Brandes, J.A., Diaz, J.M., de Jonge, M.D., Paterson, D., McNulty, I., Elliott, W.C., Northrup, P., 2011. Phosphorus K-edge XANES spectroscopy of mineral standards. Synchrotron Radiation 18 (2), 189–197.
Jackson, C.M., Nicholson, P.T., 2010. Provenance of some glass ingots from the Uluburun shipwreck. J. Archaeol. Sci. 37, 295–301.
Jollivet, P., Gin, S., Schumacher, S., 2012. Forward dissolution rate of silicate glasses of nuclear interest in clay-equilibrated groundwater. Chem. Geol. 330, 207–217.
Kamino, K., 2013. Mini-review: barnacle adhesives and adhesion. Biofouling 29 (6), 735–749.

Lin, Y.P., Singer, P.C., 2006. Inhibition of calcite precipitation by orthophosphate: speciation and thermodynamic considerations. Geochem. Cosmochim. Acta 70 (10), 2530–2539.
Ma, T., Jivkov, A.P., Li, W., Liang, W., Wang, Y., Xu, H., Han, X., 2017. A mechanistic model for long-term nuclear waste glass dissolution integrating chemical affinity and interfacial diffusion barrier. J. Nucl. Mater. 486, 70–85.
Maeda, T., Banba, T., Sonoda, K., Inagaki, Y., Furuya, H., 2001. Release and retention of uranium during glass corrosion. J. Nucl. Mater. 298 (1–2), 163–167.
Mansfield, J.T., Thorpe, C.L., Corkhill, C.L., Harrison, M.T., Hand, R.J., 2023. Localised extended ("vermiform") features formed during glass dissolution. J. Non-Cryst. Solids 608, 122230.
Martin-Diaconescu, V., Gennari, M., Gerey, B., Tsui, E., Kanady, J., Tran, R., Pécaut, J., Maganas, D., Krewald, V., Gouré, E., Duboc, C., 2015. Ca K-edge XAS as a probe of calcium centers in complex systems. Inorg. Chem. 54 (4), 1283–1292.
McCloy, J.S., 2019. Frontiers in natural and un-natural glasses: an interdisciplinary dialogue and review. J. Non-Cryst. Solids 4, 100035.
McKeown, D.A., Gan, H., Viragh, C., Pegg, I.L., 2024. X-ray absorption spectroscopic studies of Fe environments in borosilicate waste glasses synthesized under a variety of redox conditions. J. Non-Cryst. Solids 627, 122812.
Michelin, A., Burger, E., Rebiscoul, D., Neff, D., Bruguier, F., Drouet, E., Dillmann, P., Gin, S., 2013. Silicate glass alteration enhanced by iron: origin and long-term implications. Environ. Sci. Technol. 47 (2), 750–756.
Miller, W.M., Chapman, N., McKinley, I., Alexander, R., Smellie, J.A.T., 2011. Natural analogue studies in the geological disposal of radioactive wastes. Book Series: Stud. Environ. Sci. 57.
Morris, D., Andres, O., Ayers, R., Brown, A., Capuzzo, E., Cooper, K., Dye, S., Fernand, L., Flatman, S., Greenwood, N., Haverson, D., Hull, T., Hyder, K., Jennings, S., Jolliffe, R., Metcalfe, J., Meadows, B., Pearce, D., Pinnegar, J., Sophie, P., Righton, D., Taylor, N., Williams, O., Wright, S., 2016. Seawater temperature records for the UK shelf - "all" cefas seawater temperature data 1880 - 2014. Cefas, UK. V1. https://doi.org/10.14466/CefasDataHub.4.
Neeway, J.J., Rieke, P.C., Parruzot, B.P., Ryan, J.V., Asmussen, R.M., 2018. The dissolution behavior of borosilicate glasses in far-from equilibrium conditions. Geochim. Cosmochim. Acta 226, 132–148.
Nuclear Waste Services, 2023. Guide to reference groundwater and porewater compositions in support of the UK GDF programme report number: NWS-CR-23-007. https://assets.publishing.service.gov.uk/media/6569f2879462260013c5684a/NWS-CR-23-007_-_Guide_to_Reference_Groundwater_and_Porewater_Compositions_in_Support_of_the_UK_GDF_Programme.pdf. June 2024.
Ortega-Feliu, I., Gomez-Tub, B., Respaldiza, M.A., Capel, F., Nieto-Prieto, X., 2016. X-ray and gamma-ray based spectroscopic analysis of a millefiori Roman glass fragment: degradation of sunken glass from a shipwreck. J. Anal. Atomic Spectrom. 31, 773.
Palchik, N.A., Grigorieva, T.N., Moroz, T.N., 2013. Composition, structure, and properties of iron-rich nontronites of different origins. Crystallogr. Rep. 58, 302–307.
Palomar, T., 2018. Characterization of the alteration processes of historical glasses on the seabed. Mater. Chem. Phys. 214, 391e401.
Palomar, T., Llorente, I., 2016. Decay processes of silicate glasses in river and marine aquatic environments. J. Non-Cryst. Solids 449, 20–28.
Parruzot, B., Jollivet, P., Rébiscoul, D., Gin, S., 2015. Long-term alteration of basaltic glass: mechanisms and rates. Geochem. Cosmochim. Acta 154, 28–48.
Perez, A., Rossano, S., Trcera, N., Huguenot, D., Fourdrin, C., Verney-Carron, A., van Hullebusch, E.D., Guyot, F., 2016. Bioalteration of synthetic Fe (III)-, Fe (II)-bearing basaltic glasses and Fe-free glass in the presence of the heterotrophic bacteria strain Pseudomonas aeruginosa: impact of siderophores. Geochem. Cosmochim. Acta 188, 147–162.
Poinssot, C., Gin, S., 2012. Long-term behavior science: the cornerstone approach for reliably assessing the long-term performance of nuclear waste. J. Nucl. Mater. 420, 182–192.
Prietzel, J., Klysubun, W., Hurtarte, L.C.C., 2021. The fate of calcium in temperate forest soils: a Ca K-edge XANES study. Biogeochemistry 152 (2), 195–222.
Qian, Y., Scheinost, A.C., Grangeon, S., Greneche, J.M., Hoving, A., Bourhis, E., Maubec, N., Churakov, S.V., Fernandes, M.M., 2023. Oxidation state and structure of Fe in nontronite: from oxidizing to reducing conditions. ACS Earth Space Chem. 7 (10), 1868–1881.
Redknap, M., Freestone, I.C., Vlierman, K., 1995. Eighteenth-century glass ingots from England: further light on the post-medieval glass trade. In: Occasional Paper 109, Trade and Discovery: the Scientific Study of Artefacts from Post-medieval Europe and beyond. British Museum Press.
Reijonen, H.M., Alexander, W.R., Norris, S., 2023. Resilience in knowledge management–the case of natural analogues in radioactive waste management. Process Saf. Environ. Prot. 180, 205–222.
Sessegolo, L., Verney-Carron, A., Ausset, P., Nowak, S., Triquet, S., Saheb, M., Chabas, A., 2020. Alteration rate of medieval potash-lime silicate glass as a function of pH and temperature: a low pH-dependent dissolution. Chem. Geol. 550, 119704.
Silvestri, A., Molin, G., Salviulo, G., 2005. Archaeological glass alteration products in marine and land-based environments: morphological, chemical and microtextural characterization. J. Non-Cryst. Solids 351, 1338–1349.
Silvestri, A., Molin, G., Salviulo, G., 2008. The colourless glass of Iulia Felix, J. Archaeol. Sci. 35, 331e341.
Sowrey, F.E., Skipper, L.J., Pickup, D.M., Drake, K.O., Lin, Z., Smith, M.E., Newport, R.J., 2004. Systematic empirical analysis of calcium–oxygen coordination environment by calcium K-edge XANES. Phys. Chem. Chem. Phys. 6 (1), 188–192.
Strachan, D.M., Crum, J.V., Ryan, J.V., Silvestri, A., 2014. Characterization and modeling of the cemented sediment surrounding the Iulia Felix glass. Appl. Geochem. 41, 107–114.
Strachan, D.M., 2001. Glass dissolution: testing and modeling for long-term behavior. J. Nucl. Mater. 298 (1–2), 69–77.
Stroncik, N.A., Schmincke, H.U., 2001. Evolution of palagonite: crystallization, chemical changes, and element budget. G-cubed 2 (7).
Stuart, I., 1991. Glass bottles from the loch ard shipwreck (1878): a preliminary study. In: Australian Historical Archaeology, vol. 9.
Tadier, S., Rokidi, S., Rey, C., Combes, C., Koutsoukos, P.G., 2017. Crystal growth of aragonite in the presence of phosphate. J. Cryst. Growth 458, 44–52.
Techer, I., Advocat, T., Lancelot, J., Liotard, J.M., 2000. Basaltic glass: alteration mechanisms and analogy with nuclear waste glasses. J. Nucl. Mater. 282 (1), 40–46.
Thien, B., Godon, N., Hubert, F., Angéli, F., Gin, S., Ayral, A., 2010. Structural identification of a trioctahedral smectite formed by the aqueous alteration of a nuclear glass. Appl. Clay Sci. 49 (3), 135–141.
Thorpe, C.L., Neeway, J.J., Pearce, C.I., Hand, R.J., Fisher, A.J., Walling, S.A., Hyatt, N. C., Kruger, A.A., Schweiger, M., Kosson, D.S., Arendt, C.L., 2021. Forty years of durability assessment of nuclear waste glass by standard methods. npj Mater. Degrad. 5 (1), 61.
Thorpe, C.L., Crawford, R., Hand, R.J., Radford, J.T., Corkhill, C.L., Pearce, C.I., Neeway, J.J., Plymale, A.E., Kruger, A.A., Morris, K., Boothman, C., 2024. Microbial interactions with phosphorus containing glasses representative of vitrified radioactive waste. J. Hazard Mater. 462, 132667.
Valbi, V., Leplat, J., François, A., Perez, A., Trichereau, B., Ranchoux, C., Verney-Carron, A., Loisel, C., Rossano, S., 2023. Bacterial diversity on stained glass windows. Int. Biodeterior. Biodegrad. 177, 105529.
Verney-Carron, A., Sessegolo, L., Chabas, A., Lombardo, T., Rossano, S., Perez, A., Valbi, V., Boutillez, C., Muller, C., Vaulot, C., Trichereau, B., 2023. Alteration of medieval stained glass windows in atmospheric medium: review and simplified alteration model. npj Mater. Degrad. 7 (1), 49.
Verney-Carron, A., Gin, S., Libourel, G.A., 2008. Fractured roman glass block altered for 1800 years in seawater: analogy with nuclear waste glass in a deep geological repository. Geochem. Cosmochim. Acta 72, 5372–5385.
Verney-Carron, A., Gin, S., Frugier, P., Libourel, G., 2010. Long-term modeling of alteration-transport coupling: application to a fractured Roman glass. Geochem. Cosmochim. Acta 74, 2291e2315.
Weaver, J.L., DePriest, P.T., Koestler, R.J., 2021. Microbial interactions with silicate glasses. npj Mater. Degrad. 5, 1.
Wilke, M., Farges, F., Petit, P.E., Brown Jr, G.E., Martin, F., 2001. Oxidation state and coordination of Fe in minerals: an Fe K-XANES spectroscopic study. Am. Mineral. 86 (5–6), 714–730.
Wilke, M., Partzsch, G.M., Bernhardt, R., Lattard, D., 2004. Determination of the iron oxidation state in basaltic glasses using XANES at the K-edge. Chem. Geol. 213 (1–3), 71–87.
Wilke, M., Farges, F., Partzsch, G.M., Schmidt, C., Behrens, H., 2007. Speciation of Fe in silicate glasses and melts by in-situ XANES spectroscopy. Am. Mineral. 92 (1), 44–56.